Dear author,

Please note that changes made in the online proofing system will be added to the article before publication but are not reflected in this PDF.

We also ask that this file not be used for submitting corrections.

Lithos xxx (xxxx) xxx

Contents lists available at ScienceDirect

Lithos

journal homepage: www.elsevier.com/locate/lithos

Age and geochemistry of the Beata Ridge: Primary formation during the main phase (~89 Ma) of the Caribbean large Igneous Province

Antje Dürkefälden [a,*], Kaj Hoernle [a,b], Folkmar Hauff [a], Jo-Anne Wartho [a], Paul van den Bogaard [a], Reinhard Werner [a]

[a] GEOMAR Helmholtz Centre for Ocean Research Kiel, Wischhofstraße 1-3, Kiel 24148, Germany
[b] Institute of Geosciences, Kiel University, Ludewig-Meyn-Strasse 10, Kiel, Germany

A R T I C L E I N F O

Article history:
Received 17 August 2018
Accepted 17 December 2018
Available online xxxx

Keywords:
Caribbean
Large Igneous Provinces
Mantle plumes
Geochronology
Geochemistry

A B S T R A C T

The Caribbean Large Igneous Province (CLIP), a Cretaceous oceanic flood basalt province, presumably formed at the initiation of the Galápagos hotspot. During the M81 cruise of the German R/V METEOR, we sampled the Beata Ridge, a prominent submarine structure in the Caribbean Sea belonging to the CLIP. The ridge offers the opportunity to directly sample basement sequences of the central, submarine part of the CLIP, complementing numerous studies of accreted CLIP sequences exposed on land around the margins of this LIP. The majority of the recovered Beata Ridge samples are volcanic, implying that at least parts of the Beata Ridge were formed during a large extrusive event in contrast to previous assumptions that the structure is primarily composed of intrusive rocks. Several stratigraphically controlled profiles were sampled along the western slope of the Beata Ridge using the remotely operated vehicle (ROV) Kiel 6000 and revealed variously alternating sequences of magmatic rocks (lavas, pillow breccias, tuffs and gabbros) and sediment plains. We report new $^{40}Ar/^{39}Ar$ age and geochemical (major and trace element, Sr-Nd-Hf-Pb isotope) data for the recovered magmatic samples. Although the $^{40}Ar/^{39}Ar$ analyses display disturbed age spectra, they suggest an age range of 92.4–76.9 Ma. Thus our age data show for the first time that the Beata Ridge also formed during the main magmatic stage of the CLIP (~95–83 Ma). Previous studies suggested that the Beata Ridge was formed during a second, lower-volume magmatic phase of the CLIP (~81–71 Ma), possibly related to decompression melting during an extensional phase in the Caribbean. Most samples display relatively flat chondrite-normalized rare earth element (REE) patterns commonly observed throughout the CLIP, but light REE enriched and depleted compositions are also present. The occurrence of enriched and depleted incompatible element and radiogenic isotope signatures implies a heterogeneous mantle source region, as is observed for other LIPs worldwide. Since a high degree of geochemical variability is observed over short stratigraphic intervals within the ROV profiles, melt homogenization did not operate as effectively as commonly assumed for LIPs. Instead the plume head probably preserved some domains of enriched and depleted components, whereas most of the melts during the main stage have intermediate compositions (with flat REE patterns), representing mixtures of the enriched and depleted components.

1. Introduction

Large Igneous Provinces (LIPs), including continental and oceanic flood basalts, represent the largest magmatic events on Earth with erupted volumes of ~10^5–10^7 km^3 of predominantly basaltic magma (e.g., Coffin and Eldholm, 1992; Hooper, 2000; Mahoney and Coffin, 1997). They are often located at the oldest end of hotspot tracks such as the Paraná-Etendeka flood basalts at the ends of the Tristan-Gough hotspot tracks and the Deccan flood basalts at the end of the Réunion hotspot track (Richards et al., 1989). Therefore they are commonly believed to be formed by large degrees of melting of a starting plume head marking the initial activity of a mantle plume. Many LIPs, especially continental flood basalt provinces, are emplaced over large areas (up to 2000 km in diameter) during a geologically short time span of about 2–3 Ma (e.g., Courtillot and Renne, 2003), whereas oceanic flood basalts such as the Caribbean LIP (CLIP) seem to be generated over longer time scales of 30–40 Ma with multiple magmatic pulses (e.g., Hoernle et al., 2004; Révillon et al., 2000b). Studying the geochemistry of oceanic LIPs has an advantage over the study of continental flood basalts, because magmas in oceanic settings are not contaminated by continental crustal material and thus they provide a more direct insight into the mantle source (e.g., Kerr, 2014; Kerr and Mahoney, 2007). However, oceanic flood basalt provinces are less accessible than their

* Corresponding author.
E-mail address: aduerkefaelden@geomar.de (A. Dürkefälden).

https://doi.org/10.1016/j.lithos.2018.12.021
0024-4937/

continental counterparts, especially the interior portions, and therefore, knowledge about their origin, formation, internal structure and geochemical characteristics is still limited.

The CLIP belongs to a series of major magmatic events that formed in the Cretaceous, including the Ontong Java, Manihiki, Hikurangi, Shatsky and Kerguelen plateaus (e.g., Kerr, 2014). The CLIP consists of thickened oceanic crust (up to 20 km) in the central (submarine) part of the Caribbean Plate (Colombian and Venezuelan Basins with the Beata Ridge and Lower Nicaraguan Rise (LNR) as accessible windows into the interior of the LIP; Mauffret and Leroy, 1997), as well as accreted and tectonically uplifted flood basalt sequences subaerially exposed around the margins of the Caribbean Sea and northwestern South America (Fig. 1a).

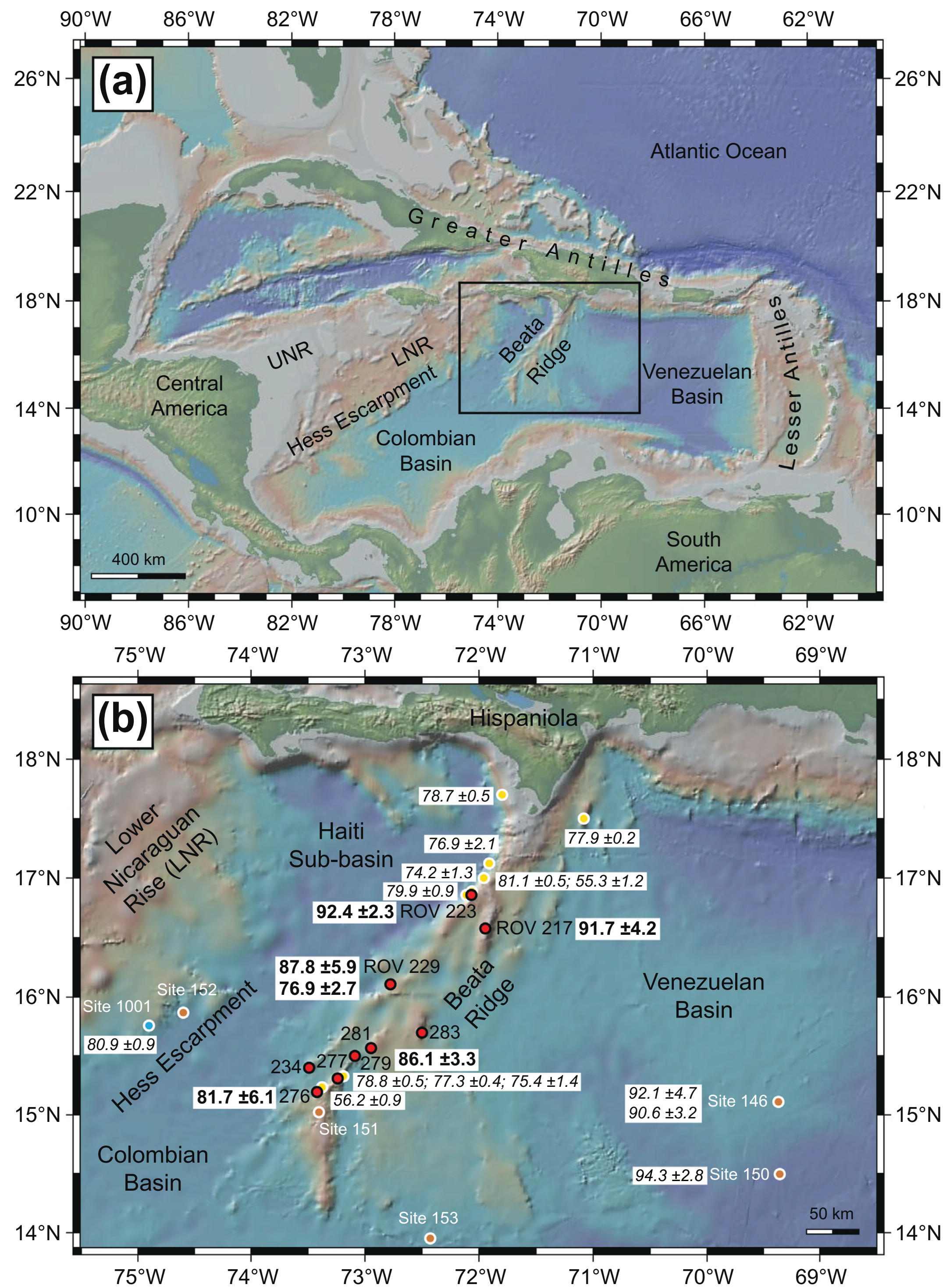

Fig. 1. (a) Overview map of the Caribbean Region. Black box denotes the location of (b). UNR = Upper Nicaraguan Rise, LNR = Lower Nicaraguan Rise. (b) Detailed map of the Beata Ridge showing the sample locations on the Beata Ridge (red dots) with $^{40}Ar/^{39}Ar$ age data in bold from this study. ROV dives were conducted at sites 217, 223 and 229, whereas at the remaining sites, samples were collected by dredging. $^{40}Ar/^{39}Ar$ age data from Révillon et al. (2000b) are shown in italics with the sample locations (yellow dots). Also shown are the locations of DSDP Leg 15 Sites 146 and 150–153 (orange dots) and from ODP Leg 165 Site 1001 (blue dot) with $^{40}Ar/^{39}Ar$ age data (Sinton et al., 1998, 2000). All ages are reported in million years with 2σ errors. Source of the maps is GeoMapApp (http://www.geomapapp.org). (For interpretation of the references to colour in this figure legend, the reader is referred to the web version of this article.)

Remnants of these terranes can be found in Costa Rica, Panama, Colombia, Ecuador and on the islands of Gorgona, Curaçao, Aruba, Hispaniola and Jamaica (e.g., Hastie et al., 2016; Hauff et al., 2000a,b; Hoernle et al., 2004; Kerr et al., 1996a; Loewen et al., 2013; Révillon et al., 2000a; Sinton et al., 1998). The Beata Ridge is a large NNE-SSW trending horst-like bathymetric high in the Caribbean Sea. Its top is located at 2000 m water depth in the north and 4000 m in the south, and the Beata Ridge rises up to 2000 m above the surrounding abyssal plains (Fig. 1a-b). It is bordered by Hispaniola in the north and separates the Venezuelan Basin in the east from the Colombian Basin and the Haiti sub-basin in the west. The ridge has a length of ~450 km and a width of up to 300 km and is characterized by steep scarps to the west but more gentle slopes to the east (Mauffret et al., 2001).

The spatial origin of the CLIP is controversial. Most authors favor an origin in the Pacific Ocean, possibly above the Galápagos mantle plume, and subsequent emplacement between North and South America due to plate tectonic movements (e.g., Duncan and Hargraves, 1984; Hastie and Kerr, 2010; Hauff et al., 2000a,b; Hoernle et al., 2002; Pindell et al., 2011; Sinton et al., 1997, 1998). Others prefer the inter-American model, which favors formation in the west of its recent position but between the Americas (e.g., Frisch et al., 1992; Meschede and Frisch, 1998). The CLIP was originally assumed to have mainly formed within a relatively short time period at ~89 Ma (95–83 Ma) followed by a second pulse of magmatic activity at ~76 Ma (81–71 Ma; Hauff et al., 2000b; Hoernle et al., 2002, 2004; Sinton et al., 1998). Some parts of the CLIP, however, are remarkably young with the youngest ages of ~53 Ma being reported from Hispaniola (Escuder-Viruete et al., 2016), ~55 Ma from the Beata Ridge (Révillon et al., 2000b) and ~62 Ma from Curaçao (Loewen et al., 2013) suggesting long-term magmatic activity to form the CLIP. The young ages, however, should be treated with caution, since they may represent later resetting of older crystallization ages during magmatic, tectonic or hydrothermal events.

Whereas the subaerial terranes of the CLIP have been extensively sampled, only limited data are available for the submarine parts, mainly by drilling during DSDP Leg 15, Sites 146 and 150–153 (Donnelly et al., 1973; Hauff et al., 2000a; Sinton et al., 1998) and ODP Leg 165, Site 1001 (Kerr et al., 2009; Sigurdsson et al., 1997; Sinton et al., 2000), and sampling of the Beata Ridge by submersible (Révillon et al., 2000b; Fig. 1b). ^{40}Ar/^{39}Ar age data of Beata Ridge samples reported by Révillon et al. (2000b) range from ~81 to ~55 Ma with none of the dated samples having ages falling within the main CLIP phase at 95–83 Ma. Despite the large age range of ~26 Ma, the dated samples from Révillon et al. (2000b) have largely uniform geochemical compositions similar to samples from the main CLIP stage with flat chondrite-normalized REE patterns. DSDP Site 151 on the southern Beata Ridge is the only other location that had been sampled thus far. The recovered basaltic rock shows a geochemically enriched composition, but age dating was not possible.

In 2010 we conducted a representative sampling of the Beata Ridge during cruise M81/2 of the German R/V Meteor. During Leg A we utilized the ROV Kiel 6000 to sample the northern and central parts, whereas during Leg B we collected samples by dredging from the southern part of the structure. We provide new ^{40}Ar/^{39}Ar ages, and geochemical (major and trace element and Sr-Nd-Hf-Pb double spike (DS) isotope) data. We show that formation of the Beata Ridge started during the main CLIP event at ~89 Ma, earlier than previously recognized, and we could not confirm ages younger than 77 Ma. Furthermore, our samples reveal a high geochemical variability including depleted and enriched compositions, in contrast to previous studies.

2. Analytical methods

2.1. Sample preparation

Sample preparation for geochemical analysis is similar to that described in Dürkefälden et al. (revised). For ^{40}Ar/^{39}Ar age dating, the freshest plagioclase crystals were hand-picked under a binocular microscope from the 0.25–0.5 mm size fraction. The picked plagioclase crystals were etched in 5% hydrofluoric acid for 8–12 min to remove surficial alteration and adhering matrix. The minerals were subsequently washed and cleaned in deionized water using an ultrasonic stick.

2.2. ^{40}Ar/^{39}Ar age dating

Six plagioclase separates were analyzed using the ^{40}Ar/^{39}Ar laser step-heating technique at the GEOMAR Geochronology Laboratory. A detailed description of the ^{40}Ar/^{39}Ar analytical methods can be found in Homrighausen et al. (2019) and references therein. The samples were irradiated in the cadmium shielded RODEO P3 position of the HFR facilities (NRG, Petten, The Netherlands) for 12 h. The fast neutron flux was monitored using Taylor Creek Rhyolite sanidine (TCR-2: 27.87 ± 0.04 Ma; 1σ; M.A. Lanphere, pers. comm.).

The average extraction system blank values obtained during the unknown sample analyses (determined after every 5 unknown analyses) were 1.07×10^{-13}, 4.33×10^{-13}, 4.69×10^{-14}, 1.03×10^{-13}, and 1.06×10^{-12} cm^3 STP (standard temperature and pressure) for ^{36}Ar, ^{37}Ar, ^{38}Ar, ^{39}Ar, and ^{40}Ar, respectively. The mass spectrometer sensitivity, mass discrimination and nuclear interference reaction correction factors are listed in Appendix A. Errors are quoted at the 2σ confidence level. The age spectra, inverse isochron plots, analytical data tables, and J values and errors for each unknown sample are noted in the ^{40}Ar/^{39}Ar data tables (Appendix A).

2.3. Major and trace elements and Sr-Nd-Pb-Hf radiogenic isotopes

All geochemical methods are described in detail in Dürkefälden et al. (revised). In summary major elements were determined by XRF and trace elements by solution ICP-MS. Results of international rock standards are provided in Appendix B, Tables B.1-3, results of analytical precision estimated from sample replicates and of instrument stability in Appendix B, Tables B.4-5.

Sr-Nd-Pb isotope analyses were conducted by thermal ionization mass spectrometry (TIMS) and Hf on a Nu plasma multicollector ICP-MS (MC-ICP-MS). Sample data are reported relative to ^{87}Sr/^{86}Sr = 0.710250 ± 0.000008 (2 standard deviation (SD); $n = 28$) for NBS987, ^{143}Nd/^{144}Nd = 0.511850 ± 0.000006 (2SD; $n = 89$) for La Jolla and ^{143}Nd/^{144}Nd = 0.511715 ± 0.000007 (2SD; $n = 11$) for our in-house SPEX Nd. Double-spike corrected NBS981 values are ^{206}Pb/^{204}Pb = 16.9432 ± 0.0026, ^{207}Pb/^{204}Pb = 15.5005 ± 0.0026 and ^{208}Pb/^{204}Pb = 36.7284 ± 0.0062 (2SD; $n = 19$). Our in-house SPEX Hf ICP standard solution (lot #9) was normalized to JMC475 with ^{176}Hf/^{177}Hf = 0.282163 leading to an average standard bracketing normalized ratio of ^{176}Hf/^{177}Hf = 0.282170 ± 0.000006 (2SD; $n = 502$).

3. Results

3.1. Sampling and ROV observations

Using the ROV Kiel 6000, we sampled magmatic rocks (pillow lavas and pillow breccias, sheet lavas, intrusive rocks and volcaniclastic rocks) along three up-slope profiles on the northwestern flanks of the northern and central Beata Ridge (ROV 217, 223 and 229; Fig. 1b). ROV profiles 220 and 226 only yielded sediments (mudstones and carbonates). Additionally, we sampled the southern part of the structure by dredging at six locations. The recovered rocks comprise basaltic, gabbroic and doleritic rocks.

Bathymetry and ROV dives display a series of en echelon step faults along the western flanks of the Beata Ridge, and the rocks show structural evidence of extensive tectonic processes. The ridge forms a horst with the Haiti sub-basin forming a graben at its western boundary.

The LNR forms another horst on the western boundary of the Haiti sub-basin (Dürkefälden et al., revised; Mauffret et al., 2001). Sampling also indicates that the Beata Ridge is still tectonically active, since we found signs of very young faulting and fluid venting (Werner et al., 2011).

Along the ROV 223 and ROV 229 profiles, we sampled several different tuffs. Some are heterogeneous and composed of clasts in a fine-grained matrix and some are lapilli tuffs comprising clasts and fine lapilli in a very fine-grained matrix. Two of the lapilli tuffs comprise a small amount of accretionary lapilli embedded in a very fine-grained ashy matrix (Werner et al., 2011; Fig. 2). Accretionary lapilli form subaerially, near vent during explosive volcanic eruptions, thus the occurrence of accretionary lapilli indicates that at least parts of the CLIP formed under subaerial conditions.

In the sections below, the profiles are described in more detail and shown in Fig. 3a-c and the sampled rocks are classified as "in situ", "non in situ" and "in situ?". "In situ" samples were broken off the outcropping rocks. "Non in situ" samples were recovered from the debris and thus may be derived from above. "In situ?" samples were loose samples collected from the outcrop or cliff and therefore are assumed quasi in situ, but not in strict sense. "Soft sediments" are loose sediments that blanket the slopes, whereas the solidified sediment layers in sequence 4 of ROV profile 223 are part of the stratigraphy (Fig. 3b).

3.1.1. ROV 217 dive

The ROV 217 dive comprised a profile of ~450 m in ~1300-840 m water depth at the upper western slope of a ridge-like structure on the northern Beata Ridge (Fig. 3a). Sequence 1 (1304-1078 m below sea level (b.s.l.)) is a pillow lava sequence with pillow breccias at the bottom and the top, and six medium-grained basaltic samples were collected (#1–6). Sequence 2 (1078-882 m b.s.l.) consists of massive lavas partly covered by soft sediments, knobbly sheet-like crust and scree. Five medium-grained basaltic samples were taken from the outcrops and from the debris (#7–11). Sequence 3 (882–843 m b.s.l.) is dominated by pillow lavas and was sampled by collecting a doleritic rock from the debris (#12) and a medium-grained basaltic rock from a massive outcrop (#13).

3.1.2. ROV 223+226 dives

The ROV 223 dive started in ~3400 m water depth on the northwestern flank of the northern Beata Ridge about 35 km NNW of the previous ROV 217 dive and sampled a profile of ~1000 m (Fig. 3b). Sequence 1 (~3420-3160 m b.s.l.) consists of massive boulder-sized scree where two gabbroic rocks were collected (#1–2), followed by a fairly steep slope with soft sediment plains and interspersed outcrops of massive rocks. Three in situ rocks, a basaltic rock (#3), a volcaniclastic breccia (#4) and a gabbro (#5), were sampled. Sequence 2 (~3160-2920 m b.s.l.) was composed of soft sediment plains, scree and structures, which according to their appearance may be lava flows, but no samples could be obtained. Sequence 3 (~2920-2760 m b.s.l.) had a very steep morphology and a gabbroic sample (#6) and a fine-grained lava (#7) were collected from the outcropping rock cliffs. Then the slope became more gentle and was covered by soft sediments and scree interrupted by some lobe-like outcrops perpendicular to the slope. From the debris field of one of these outcrops, a fine-grained tuff sample with accretionary lapilli was collected (#8). Sequence 4 (~2760-2640 m b.s.l) consists of near vertical sediment layers and scree, and a heterogeneous tuff (#9) and two solidified turbidites (#11–12) were sampled from the debris, whereas another heterogeneous tuff (#10) was sampled from the vertical sediment layers. In 2640 m water depth, an aphyric lava from a pillow lava outcrop was collected (#13). Above this outcrop the slope was covered by soft sediments (sequence 5, ~2640-2383 m b.s.l.). The ROV 226 dive was a continuation of the previous ROV 223 dive in 2369-1870 m water depth and yielded sediments and carbonates but no magmatic rocks.

3.1.3. ROV 229 dive

The ROV 229 dive was carried out at the northwestern flank of the central Beata Ridge about 100 km SW of the ROV 223 dive in ~4200–2500 m water depth resulting in a ~1700 m profile (Fig. 3c). Sequence 1 (~4201–3770 m b.s.l.) consists of massive rocks partly covered by soft sediments. Eight pieces of rock were sampled at decreasing water depth: a gabbroic rock (#1), a basaltic lava (#2), two olivine-rich basaltic rocks (#3–4), a basalt (#5), a heterogeneous tuff (#6) and two lapilli tuffs (#7–8). Between 3910 and 3770 m water depth, the slope was covered by soft sediments and scree. The first samples collected from sequence 2 (~3770–3250 m b.s.l.) were a lava clast (#9), a tuff with accretionary lapilli (#10) and a heterogeneous tuff (#11). Further up-slope, soft sediment plains alternated with massive or pillow-like rocks and scree, and three samples including two olivine-rich lavas (#12–13) and a gabbroic rock (#14) were recovered. Sequence 3 (~3250–2830 m b.s.l.) comprises sheet flows partly covered by soft sediments, and two olivine-rich lava samples (#15–16) and another lava sample (#17) were collected. The remaining part of the sequence

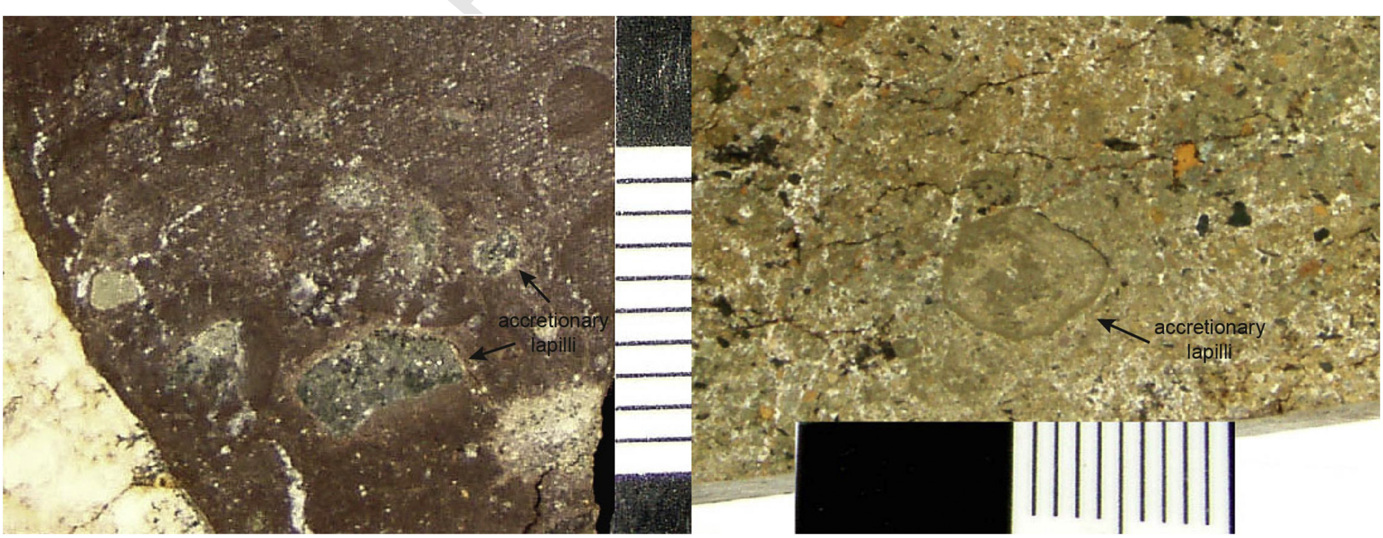

Fig. 2. Photographs showing parts of accretionary lapilli tuffs sampled during the ROV dives (Werner et al., 2011). (a) Sample 223–8 (ROV profile 223). The lapilli are 3–6 mm in diameter and composed of a core, which is surrounded by a < 1 mm thick rim of dark red, fine-grained ash. (b) Sample 229–10 (ROV profile 229). The lapilli are rounded, up to 8 mm in diameter and consist of a core of coarser grained ash surrounded by a rim of compositionally similar, very fine-grained, ash. White scale = 1 cm. (For interpretation of the references to colour in this figure legend, the reader is referred to the web version of this article.)

Please cite this article as: A. Dürkefälden, K. Hoernle, F. Hauff, et al., Age and geochemistry of the Beata Ridge: Primary formation during the main phase (~89Ma) of the Cari..., Lithos, https://doi.org/10.1016/j.lithos.2018.12.021

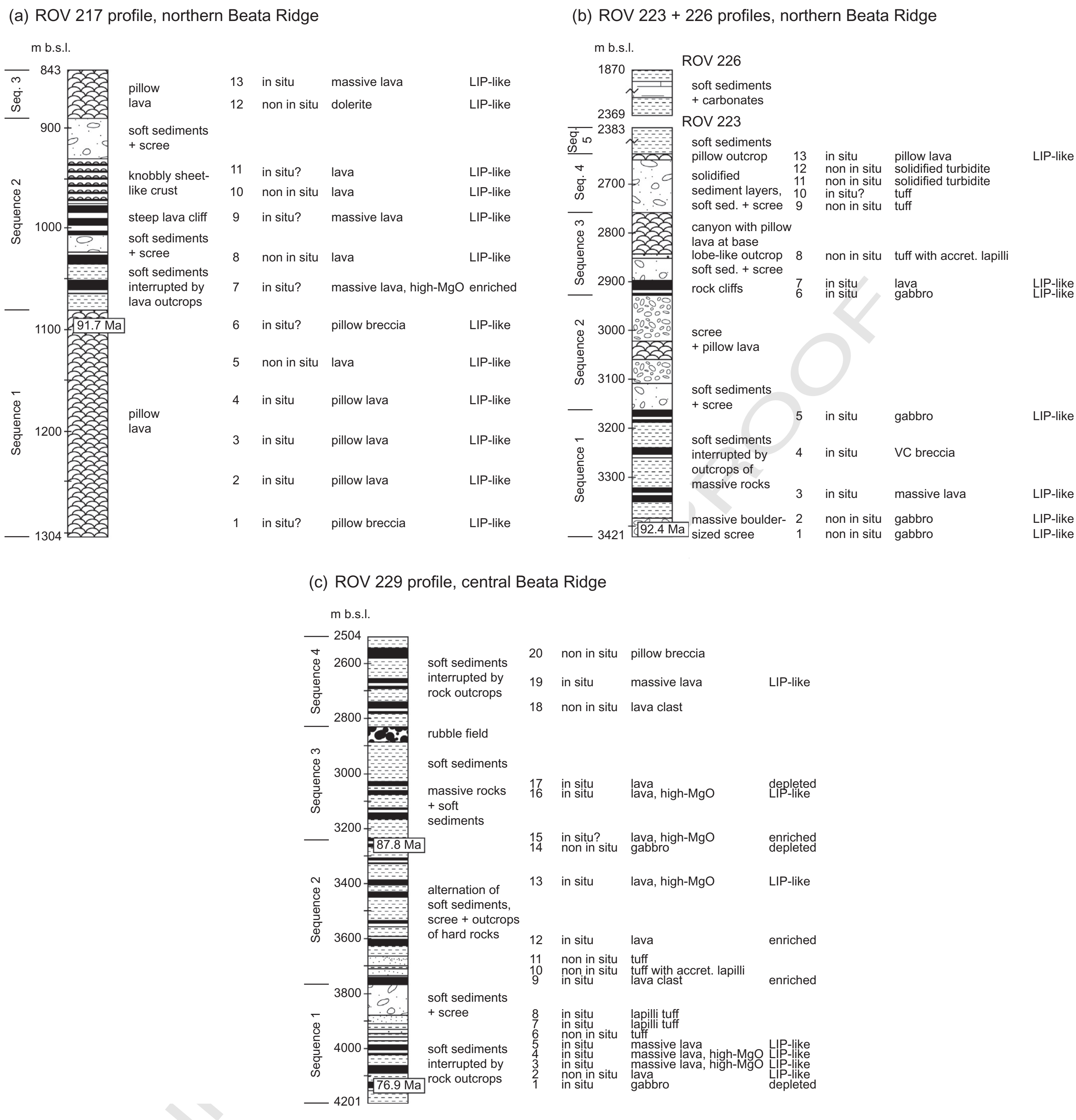

Fig. 3. (a) ROV 217 profile and (b) ROV 223 + 226 profiles from the northern Beata Ridge, and (c) ROV 229 profile from the central Beata Ridge. The profiles were recorded and sampled during ROV dives on the SW flanks of the ridge. Also listed are the collected samples including their origin (in situ – non in situ), rock type and trace element compositions. In situ? = collected directly at the base of an outcrop and therefore assumed to be quasi in situ; accret. = accretionary.

consists of a steep slope covered with soft sediments and a rubble field. From sequence 4 (2830–2504 m b.s.l.), two lava clasts (#18–19) and a pillow breccia (#20) were sampled.

3.1.4. Dredging

Two parallel, NW-SE trending ridge-like structures and two seamounts in the southern part of the Beata Ridge were sampled by dredging in ~3800–1640 m water depth. Dredge tracks at four locations on the ridges recovered lavas, gabbroic rocks and volcanic breccias (dredge 234), lavas and gabbroic rocks (dredge 276) and lava fragments (dredges 277 and 279). Sampling of an elongated, ridge-like seamount to the northeast of these structures revealed lava fragments and doleritic rocks (dredge 281), and dredge 283 conducted at an elongated seamount about 60 km further east recovered lavas and dolerites (Fig. 1b).

3.2. Petrography

Most of the basaltic samples are aphyric, but some show a porphyritic texture with plagioclase and/or clinopyroxene phenocrysts (≤1.5 mm) in a fine- to medium-grained groundmass consisting of plagioclase, clinopyroxene, magnetite and chrome-spinel. Vesicles in some samples were filled with alteration phases such as zeolite and calcite. Gabbroic rocks are coarse-grained and doleritic rocks are medium-grained and both types contain the same mineral assemblage as the basaltic samples. All rocks are moderately to strongly altered and usually coated with a 1–3 mm thick manganese crust.

Interestingly, a subset of samples shows picritic characteristics. These samples consist of ~15–35% olivine pseudomorphs up to 3 mm in size in a fine-grained groundmass composed of plagioclase, clinopyroxene and Fe—Ti oxides. The olivine in most samples is completely replaced by iddingsite, resulting in a reddish to brownish colour, and the olivine in one sample is altered to serpentinite. These samples have much higher MgO contents (12.4–18.6 wt%) than the basaltic samples (3.8–9.7 wt%).

3.3. ^{40}Ar/^{39}Ar age dating

Four plagioclase samples from the Beata Ridge generated plateau ages, whereas sample 223–1 gives a pseudo-plateau (40–49% ^{39}Ar), and sample 276–8 gives a high-temperature weighted mean age (Table 1). All the samples, however, are highly affected by alteration showing disturbed age spectra, and variable ^{36}Ar/^{37}Ar alteration index values and % atmospheric ^{40}Ar concentrations. The low wt% K contents of some of the rocks and plagioclase separates (0.03–0.28 wt% for the plagioclases; Appendix A) resulted in some large step errors, and in all samples (except sample 217–6) the Ca/K ratios suggest the presence of mixed phases in the plagioclase separates. For these reasons, the ^{40}Ar/^{39}Ar ages of these samples should be treated with caution. The inverse isochron ages are statistically invalid for some samples, however, the initial ^{40}Ar/^{36}Ar ratios are within error of the ^{40}Ar/^{36}Ar ratio of air and the inverse isochron ages overlap (within 95% confidence limit) with the plateau ages, thus giving us some confidence in these plateau, pseudo-plateau and weighted mean ages (Appendix A).

Basaltic sample 217–6 from the northern part of the Beata Ridge shows a plateau age of 91.7 ± 4.2 Ma (2σ, Mean Square Weighted Deviation (MSWD) = 0.7, Probability (P; fraction) = 0.76, 100% ^{39}Ar released). All the steps (1–15) were used for plateau age determination, but only steps 10 and 12–13 were obtained from fresh material (i.e., have low ^{36}Ar/^{37}Ar AI values of <0.00006). The statistically invalid inverse isochron age is 90.4 ± 3.9 Ma (95% conf., MSWD = 2.4, P = 0.00, Spreading Factor (SF) = 95.6%) but the initial ^{40}Ar/^{36}Ar = 296.7 ± 1.4 is within error of air, and the inverse isochron age is within error of the plateau age.

Sample 223–1, a gabbro also recovered from the northern Beata Ridge, yields a pseudo-plateau age of 92.4 ± 2.3 Ma (2σ, MSWD = 0.6, P = 0.82, 40.9% ^{39}Ar released). The sample has a U-shaped age spectrum and steps 5–15 were used to calculate the pseudo-plateau age, but none of the steps are from fresh material (i.e., all steps have high ^{36}Ar/^{37}Ar AI values). Calculation of the inverse isochron age gives an age of 93.6 ± 2.8 Ma (95% conf., MSWD = 2.2, P = 0.02, SF = 59.5%, initial ^{40}Ar/^{36}Ar = 291.3 ± 7.0), which is statistically invalid due to a P value of <0.05, but the initial ^{40}Ar/^{36}Ar ratio is within error of air, and the pseudo-plateau and inverse isochron ages overlap.

Gabbroic sample 229–1, from the central part of the Beata Ridge, yields a plateau age of 76.9 ± 2.7 Ma (2σ) calculated from steps 3–16 (MSWD = 0.8, P = 0.65, 64.4% ^{39}Ar released), but all steps are from altered material (i.e., all steps have high ^{36}Ar/^{37}Ar AI values) and the spectrum is also U-shaped. The inverse isochron age of 79.7 ± 6.2 Ma (95% conf., MSWD = 3.2 and P = 0.00, SF = 45.8%, initial ^{40}Ar/^{36}Ar = 291.9 ± 7.4) is statistically invalid due to a P value of <0.05, but the initial ^{40}Ar/^{36}Ar is within error of the atmospheric ratio, and the inverse isochron age overlaps with the plateau age.

Another gabbroic sample, 229–14, from the central Beata Ridge region gives a plateau age of 87.8 ± 5.9 Ma (2σ, MSWD = 1.2, P = 0.31, 72.2% ^{39}Ar released) and displays a staircase age spectrum. Steps 6–16 were used to determine the plateau age and steps 10–16 are derived from fresh material (i.e., low ^{36}Ar/^{37}Ar AI values). The sample has a statistically invalid inverse isochron age of 90.7 ± 8.4 Ma (95% conf., MSWD = 4.3 and P = 0.00, SF = 83.2%, initial ^{40}Ar/^{36}Ar = 281 ± 24) due to a low P value of <0.05, but the initial ^{40}Ar/^{36}Ar ratio is within error of the atmospheric ratio, and the inverse isochron agrees with the plateau age.

Gabbroic sample 276-8 from the southern Beata Ridge yields a high-temperature weighted mean age of 81.7 ± 6.1 Ma (2σ, MSWD = 1.8, P = 0.10, steps 10–15). Although this sample has a disturbed U-shaped age spectrum, the ^{36}Ar/^{37}Ar alteration index values of the high-temperature steps 10–15 show that they originate from fresh or nearly fresh material. The inverse isochron age of 100 ± 27 Ma (95% conf., MWSD = 4.6, P = 0.001, SF = 47.8%, initial ^{40}Ar/^{36}Ar = 221 ± 75) from steps 10–15 is statistically invalid due to low P and shows large errors both in the age and initial ^{40}Ar/^{36}Ar ratio due to some clustering of the data. The inverse isochron data, however, does agree within error with the ^{40}Ar/^{36}Ar atmospheric ratio and the high-temperature weighted mean age.

Basaltic sample 279–1 from the southern part of the Beata Ridge yields a plateau age of 86.1 ± 3.3 Ma (2σ, MSWD = 1.2, P = 0.27,

Table 1
^{40}Ar/^{39}Ar laser step-heating results from the Beata Ridge including plateau, pseudo-plateau, weighted mean ages (WMA) and inverse isochron ages. All ages were determined on plagioclase separates (0.25–0.5 mm). MSWD = Mean Square Weighted Deviation, P = Probability (fraction), SF = Spreading Factor. The full ^{40}Ar/^{39}Ar tables for each sample are shown in Appendix A.

Weighted mean ages

Sample	Rock type	Lab No	Age (Ma)	±	2σ (Ma)	Age type	MSWD	Prob.	^{39}Ar fraction	Steps	% atmos. ^{40}Ar range	Steps with fresh material	wt% K (from ^{39}Ar$_K$)
M81–217-6	Basalt	217–6fss	91.7	±	4.2	Plateau	0.7	0.76	100.0	1 to 15	0–99	10, 12 to 13	0.03
M81–223-1	Gabbro	223–1fss	92.4	±	2.3	Pseudo-plateau	0.6	0.82	40.9	5 to 15	16–92	None	0.28
M81–229-1	Gabbro	229–1fss	76.9	±	2.7	Plateau	0.8	0.65	64.4	3 to 16	36–96	None	0.16
M81–229-14	Gabbro	229–14fss	87.8	±	5.9	Plateau	1.2	0.31	72.2	6 to 16	0–98	10 to 16	0.04
M81–276-8	Gabbro	276–8fss	81.7	±	6.1	WMA	1.8	0.10	–	10 to 15	1–98	13 to 15	0.05
M81–279-1	Basalt	279–1 fs2	86.1	±	3.3	Plateau	1.2	0.27	100.0	1 to 16	26–80	None	0.03

Inverse isochron ages ±95% conf.

Sample	Rock type	Lab No	Age (Ma)	±	2σ (Ma)	Initial ^{40}Ar^{36}Ar	MSWD	Prob.	SF (%)	Steps
M81–217-6	Basalt	217–6fss	90.4	±	3.9	296.7 ± 1.4	2.40	0.00	95.6	1 to 15
M81–223-1	Gabbro	223–1fss	93.6	±	2.8	291.3 ± 7.0	2.20	0.02	59.5	5 to 15
M81–229-1	Gabbro	229–1fss	79.7	±	6.2	291.9 ± 7.4	3.20	0.00	45.8	3 to 16
M81–229-14	Gabbro	229–14fss	90.7	±	8.4	281 ± 24	4.30	0.00	83.2	6 to 16
M81–276-8	Gabbro	276–8fss	100	±	27	221 ± 75	4.60	0.00	47.8	10 to 15
M81–279-1	Basalt	279–1 fs2	87.6	±	6.6	288 ± 26	4.90	0.00	51.8	1 to 16

Please cite this article as: A. Dürkefälden, K. Hoernle, F. Hauff, et al., Age and geochemistry of the Beata Ridge: Primary formation during the main phase (~89Ma) of the Cari..., Lithos, https://doi.org/10.1016/j.lithos.2018.12.021

100% ^{39}Ar released). The age was calculated from steps 1–16, but the $^{36}Ar/^{37}Ar$ alteration index values indicate that all steps are derived from altered material. The inverse isochron age is 87.6 ± 6.6 Ma (95% conf., MSWD = 4.9, P = 0.00, SF = 51.8%, initial $^{40}Ar/^{36}Ar$ = 288 ± 26) and is statistically invalid due to high MSWD and low P, but the initial $^{40}Ar/^{36}Ar$ is within error of the atmospheric ratios, and the plateau and inverse isochron ages overlap within error.

3.4. Geochemical results

3.4.1. Major and trace elements

Measured major and trace element concentrations are reported in Tables 2 and 3. Due to extensive alteration of many of the collected samples, with loss on ignition (LOI) values of up to 9.6 wt%, major element analyses are only of limited use. In particular, Na_2O, K_2O and P_2O_5 can be affected by alteration processes, as is the case with large ion lithophile trace elements, e.g. Cs, Rb, Sr. In contrast, the REEs and the high field strength elements (HFSE) such as Zr, Hf, Nb, Ta and Ti are considered to be relatively immobile in fluids during alteration processes. Therefore, we will focus on the immobile elements. For classification of our samples, we utilize the Nb/Y versus Zr/Ti diagram after Pearce (1996), and most of the samples plot well within the basalt field, but some plot within the alkali basalt field (Fig. 4). The rocks can be divided into three geochemically distinct groups with Nb/Y = 0.05–0.13 and 0.13–0.51 for the basaltic samples and Nb/Y = 0.91–2.04 for the alkalic samples.

On REE (Fig. 5) and multi-element diagrams (Fig. 6), these three groups can also be separated. The majority of samples show nearly flat patterns typical for oceanic flood basalt provinces (henceforth referred to as LIP-like) with average values of $(La/Yb)_N$ = 1.14 and $(La/Sm)_N$ = 0.89, which were recovered from a couple of sites on the Beata Ridge from north to south. Six samples have more light rare earth element (LREE) depleted patterns resembling a normal mid-ocean ridge basalt (N-MORB) pattern (average $(La/Yb)_N$ = 0.55 and $(La/Sm)_N$ = 0.59), whereas the four alkali basalt samples have an ocean island basalt (OIB)-like character with enriched LREE patterns (average $(La/Yb)_N$ = 8.84 and $(La/Sm)_N$ = 3.02; Fig. 4). Regarding the spatial distribution of geochemical characteristics, the rocks sampled on the northern Beata Ridge have largely uniform and mostly flat patterns with only one sample from the ROV 217 profile displaying enriched compositions. In contrast, the central portion of the ridge (ROV229) is very heterogeneous, varying from depleted to LIP-like to enriched compositions. The dredge samples from the southern Beata Ridge comprise LIP-like and N-MORB-like patterns but lack enriched patterns.

Table 2
Major element concentrations (wt%) from the Beata Ridge.

Sample	Lat (°)	Long (°)	Rock type	SiO_2	TiO_2	Al_2O_3	Fe_2O_3	MnO	MgO	CaO	Na_2O	K_2O	P_2O_5	SO_3	L.O.I.	Total
Beata Ridge LIP-like																
M81–217-1	16.55	−71.95	Basalt	49.66	1.27	13.57	12.09	0.18	7.28	9.87	3.41	0.30	0.10	0.04	2.35	100.12
M81–217-2	16.55	−71.95	Basalt	49.54	1.23	13.42	12.15	0.17	7.85	8.35	3.85	0.19	0.09	0.02	3.07	99.93
M81–217-3	16.55	−71.95	Basalt	48.27	1.23	13.82	12.25	0.16	7.72	9.19	3.57	0.07	0.09	0.11	3.39	99.87
M81–217-4	16.55	−71.95	Basalt	48.46	1.24	14.12	11.88	0.17	7.76	12.48	2.01	0.24	0.09	0.02	1.69	100.16
M81–217-5	16.55	−71.95	Basalt	46.98	1.19	14.96	10.74	0.13	8.34	10.40	2.19	0.59	0.09	0.02	4.28	99.91
M81–217-6	16.55	−71.95	Basalt	48.78	1.29	14.16	11.83	0.18	7.04	12.11	2.04	0.29	0.11	0.02	1.63	99.48
M81–217-8	16.55	−71.95	Basalt	47.70	1.31	14.27	11.01	0.13	8.06	11.38	1.99	0.38	0.11	0.03	2.59	98.96
M81–217-9	16.55	−71.95	Basalt	47.59	1.19	14.11	11.48	0.16	8.31	11.97	1.83	0.31	0.10	0.03	2.32	99.40
M81–217-10	16.55	−71.95	Basalt	46.87	1.37	14.92	12.15	0.15	6.75	11.41	2.30	0.37	0.13	0.02	2.63	99.07
M81–217-11	16.55	−71.95	Basalt	47.98	1.23	13.76	13.29	0.16	7.57	8.59	3.13	0.66	0.10	0.02	2.68	99.17
M81–217-12	16.55	−71.95	Dolerite	48.64	1.33	13.36	12.55	0.16	7.44	9.54	3.33	0.33	0.10	0.03	3.04	99.85
M81–217-13	16.55	−71.95	Basalt	47.54	1.53	13.48	13.69	0.13	7.65	7.42	3.79	0.31	0.14	0.09	4.52	100.29
M81–223-1	16.86	−72.10	Gabbro	46.20	0.65	19.51	5.63	0.11	6.99	14.47	1.89	0.24	0.08	0.03	2.94	98.74
M81–223-2	16.86	−72.10	Gabbro	47.28	0.78	18.40	7.56	0.12	6.64	13.85	2.04	0.23	0.06	0.02	2.29	99.27
M81–223-3	16.86	−72.10	Basalt	47.82	1.58	15.34	12.97	0.19	5.36	10.75	2.97	0.48	0.15	0.02	1.98	99.61
M81–223-5	16.86	−72.10	Gabbro	47.12	2.35	12.51	17.05	0.29	5.71	6.49	3.61	0.50	0.15	0.02	4.06	99.86
M81–223-6	16.86	−72.10	Gabbro	44.99	2.86	12.55	19.25	0.26	4.99	5.55	3.25	1.06	0.18	0.03	5.23	100.20
M81–223-7	16.86	−72.10	Basalt	49.15	0.95	14.53	9.98	0.17	7.57	11.49	2.60	0.56	0.09	0.02	2.77	99.88
M81–223-13	16.86	−72.10	Basalt	46.54	2.51	14.85	12.75	0.17	5.67	9.66	2.73	1.03	0.25	0.02	3.47	99.65
M81–229-2	16.10	−72.85	Basalt	48.47	1.37	14.15	12.39	0.17	7.70	9.27	3.48	0.36	0.10	0.02	3.24	100.72
M81–229-3	16.10	−72.85	Basalt	43.78	0.66	10.90	13.20	0.14	13.90	6.92	3.26	0.63	0.07	0.05	7.40	100.91
M81–229-4	16.10	−72.85	Basalt	42.36	0.67	10.05	11.96	0.12	16.65	6.15	1.08	0.42	0.08	0.01	9.58	99.13
M81–229-5	16.10	−72.85	Basalt	47.36	0.93	15.62	10.11	0.09	8.11	10.25	1.90	0.90	0.08	0.01	4.05	99.41
M81–229-13	16.10	−72.85	Basalt	45.93	0.90	10.88	11.25	0.14	12.20	5.17	1.41	3.38	0.13	0.01	7.49	98.89
M81–229-16	16.10	−72.85	Basalt	45.42	0.95	10.99	11.42	0.17	13.17	6.20	1.54	1.83	0.10	0.02	7.16	98.97
M81–229-19	16.10	−72.85	Basalt	48.28	1.40	14.11	12.80	0.18	6.49	11.14	2.53	0.46	0.12	0.02	2.51	100.04
M81–234-1	15.40	−73.49	Dolerite	47.55	1.00	14.23	10.28	0.15	9.03	11.03	2.73	0.66	0.08	0.02	3.01	99.77
M81–234-6	15.40	−73.49	Basalt	48.14	1.25	14.02	11.88	0.17	8.29	10.07	2.34	0.85	0.12	0.01	3.28	100.42
M81–277-3	15.31	−73.26	Basalt	47.14	1.30	15.11	11.43	0.14	7.93	10.94	2.09	0.69	0.12	0.02	3.22	100.13
M81–279-1	15.49	−73.10	Basalt	46.72	3.18	14.94	13.45	0.11	3.58	8.39	2.74	1.37	0.74	0.01	3.42	98.65
M81–281-1	15.55	−72.95	Dolerite	48.69	1.24	14.72	10.88	0.15	7.45	11.62	2.10	0.62	0.11	0.01	2.72	100.31
M81–283-4	15.71	−72.55	Basalt	48.42	1.50	14.24	13.78	0.21	6.15	11.05	2.42	0.39	0.13	0.01	1.98	100.28
M81–283-7	15.71	−72.55	Dolerite	48.52	1.44	14.48	11.64	0.16	6.70	11.86	2.27	0.46	0.13	0.01	2.12	99.79
Beata Ridge depleted																
M81–229-1	16.10	−72.85	Gabbro	46.00	1.46	15.07	18.30	0.23	5.78	6.62	3.04	0.67	0.14	0.02	3.33	100.66
M81–229-14	16.10	−72.85	Gabbro	50.40	0.54	13.24	8.40	0.17	8.49	14.73	1.82	0.43	0.05	0.02	0.96	99.25
M81–229-17	16.10	−72.85	Basalt	46.29	1.00	15.29	11.76	0.20	8.49	10.98	2.33	0.42	0.08	0.02	3.09	99.95
M81–234-4	15.40	−73.49	Basalt	48.68	1.31	15.34	12.31	0.16	6.16	11.39	2.40	0.38	0.12	0.02	1.89	100.16
M81–276-4	15.20	−73.41	Basalt	48.88	1.31	13.96	14.59	0.22	6.21	11.11	2.15	0.22	0.09	0.00	1.12	99.86
M81–276-8	15.20	−73.41	Gabbro	47.30	1.83	13.40	15.16	0.24	6.34	11.87	2.38	0.27	0.11	0.01	1.37	100.28
Beata Ridge enriched																
M81–217-7	16.55	−71.95	Alkali basalt	42.46	1.23	12.60	9.52	0.13	12.99	9.27	1.72	0.45	0.24	0.02	7.73	98.36
M81–229-9	16.10	−72.85	Alkali basalt	45.68	2.22	13.03	11.09	0.18	9.16	9.79	2.36	0.73	0.23	0.01	4.22	98.70
M81–229-12	16.10	−72.85	Alkali basalt	48.99	2.31	15.00	10.19	0.15	7.07	9.80	3.22	0.95	0.25	0.02	3.11	101.06
M81–229-15	16.10	−72.85	Alkali basalt	44.94	1.55	10.94	12.23	0.13	11.65	9.62	1.88	0.54	0.15	0.02	5.18	98.83

Please cite this article as: A. Dürkefälden, K. Hoernle, F. Hauff, et al., Age and geochemistry of the Beata Ridge: Primary formation during the main phase (~89Ma) of the Cari..., Lithos, https://doi.org/10.1016/j.lithos.2018.12.021

Table 3
Trace element concentrations (ppm) from the Beata Ridge.

Sample	Li	Sc	V	Cr	Co	Ni	Cu	Zn	Ga	Rb	Sr	Y	Zr	Nb	Cs	Ba	La	
Beata Ridge LIP-like																		
M81–217-1	10.1	46.6	345	148	44.6	79.3	139	101	14.1	5.55	175	22.8	62.3	3.78	0.113	203	3.46	
M81–217-2	14.5	48.2	324	216	45.6	90.6	136	84.3	12.8	3.18	269	20.8	55.7	3.38	0.100	144	2.89	
M81–217-3	12.3	48.7	334	191	45.6	88.0	146	104	15.6	1.21	208	22.5	58.4	3.43	0.050	29.2	3.19	
M81–217-4	22.4	53.1	362	247	56.8	120	143	88.6	16.6	4.74	112	22.3	59.2	3.46	0.326	17.0	3.00	
M81–217-4[a]	22.6	53.1	362	250	56.1	120	144	91.2	16.6	4.7	110	22.2	59.1	3.47	0.328	17.0	2.99	
M81–217-5	95.8	48.4	322	319	52.5	127	180	90.6	16.9	19.6	104	19.6	57.5	3.33	1.10	23.5	2.91	
M81–217-6	28.6	51.3	371	177	48.9	80.7	169	118	17.4	16.2	104	22.8	64.4	3.80	1.70	18.2	3.41	
M81–217-8	76.4	51.6	359	230	48.3	98.0	171	97.0	16.8	19.7	106	22.6	67.0	3.96	1.40	16.3	3.33	
M81–217-9	86.6	51.8	350	303	52.2	113	168	94.4	16.5	15.7	94.8	20.2	57.9	3.39	1.77	14.9	2.93	
M81–217-10	182	52.4	378	205	50.7	88.0	168	118	18.6	17.5	110	23.5	70.3	4.06	1.77	26.9	3.56	
M81–217-11	59.8	47.9	348	139	52.3	86.5	163	88.0	16.2	8.58	320	24.1	63.9	3.61	0.298	732	3.25	
M81–217-12	39.6	48.4	353	167	48.2	83.1	152	97.4	16.5	4.20	240	23.5	67.7	3.95	0.181	117	3.43	
M81–217-13	66.1	47.5	363	61.0	49.5	78.4	170	114	17.6	4.17	135	27.5	77.8	4.52	0.240	16.9	3.99	
M81–223-1	9.25	31.5	202	260	26.9	127	89.8	44.2	16.3	3.31	140	15.4	39.6	2.28	0.186	36.7	2.61	
M81–223-1[a]	9.25	31.0	198	257	26.6	124	88.3	42.0	16.1	3.5	138	15.2	39.6	2.22	0.185	36.4	2.61	
M81–223-2	17.4	40.1	252	430	36.4	132	150	63.1	16.5	4.07	141	12.9	35.8	2.14	0.348	19.7	1.99	
M81–223-3	16.9	48.5	392	194	39.6	76.1	193	113	19.0	9.19	221	29.6	88.9	5.37	0.307	94.0	5.17	
M81–223-5	45.7	50.2	552	9.61	49.1	55.0	120	225	20.4	11.7	149	25.5	90.0	6.93	0.910	51.9	4.66	
M81–223-6	43.5	43.4	656	6.66	55.4	54.9	182	190	21.3	15.9	80.3	27.3	119	9.09	1.43	18.4	5.24	
M81–223-7	29.9	52.7	291	26.2	35.2	68.8	152	88.7	16.9	9.70	122	21.6	51.0	3.37	0.569	64.4	3.24	
M81–223-13	34.4	42.5	376	135	48.2	76.8	216	145	21.8	17.7	299	31.7	140	10.2	1.32	52.1	8.95	
M81–229-2	10.7	45.5	323	261	45.1	103	57.5	76.4	15.3	4.74	413	20.2	26.1	3.78	0.180	39.1	3.14	
M81–229-3	88.6	38.6	222	2814	99.8	906	92.2	158	10.8	7.55	62.1	10.9	30.5	2.56	0.340	21.6	2.25	
M81–229-4	128	38.4	241	2695	78.9	873	98.0	193	10.3	7.97	45.3	11.4	29.4	2.54	0.475	13.7	1.98	
M81–229-5	48.1	49.4	289	937	46.9	264	127	114	16.1	34.1	108	13.1	43.4	3.65	2.43	25.4	3.03	
M81–229-13	54.6	45.1	248	1214	59.8	557	135	127	11.4	19.8	1381	17.9	54.9	4.58	0.303	170	5.04	
M81–229-16	39.8	47.7	260	1722	53.9	388	151	112	10.1	14.9	554	16.4	47.4	8.40	0.362	395	6.43	
M81–229-19	29.4	56.0	406	118	40.5	56.6	195	115	18.4	15.4	90.0	30.4	74.6	3.97	1.48	23.8	3.56	
M81–234-1	20.2	56.2	313	547	39.3	130	113	92.0	13.5	24.3	146	19.4	17.8	2.50	2.38	138	2.63	
M81–234-6	32.0	51.9	352	353	48.8	147	152	174	16.6	84.5	143	20.8	54.3	3.39	6.59	38.0	3.06	
M81–277-3	47.9	50.3	342	351	42.1	111	164	213	17.9	29.4	106	24.2	63.5	3.90	3.31	20.9	4.79	
M81–279-1	37.6	46.2	422	48.1	55.8	55.8	581	181	21.5	135	111	41.0	152	6.44	10.1	46.8	5.65	
M81–281-1	43.1	47.7	317	362	41.4	112	138	137	16.3	16.7	109	21.7	62.6	3.90	1.13	24.0	3.44	
M81–283–4	21.8	52.2	395	130	45.9	65.6	164	137	19.0	15.9	108	26.9	74.4	4.23	1.18	16.2	3.68	
M81–283-7	21.9	52.9	388	233	53.1	89.4	111	99.6	18.7	10.6	111	26.2	72.6	4.17	0.573	16.8	3.75	
Beata Ridge depleted																		
M81–229-1	44.3	25.1	440	5.23	66.0	83.4	216	119	19.2	13.3	152	28.4	44.8	2.37	0.520	49.8	2.59	
M81–229-14	14.0	78.9	314	19.5	39.3	74.9	122	63.0	13.2	6.09	69.7	11.6	20.1	0.791	0.406	7.43	0.944	
M81–229-14[a]	14.1	79.9	321	19.7	39.2	75.6	122	64.0	13.4	6.14	70.9	11.6	20.1	0.784	0.403	7.44	0.954	
M81–229-17	30.4	51.1	308	329	49.5	128	181	95.7	15.7	8.85	233	24.6	45.6	1.15	0.891	44.2	1.77	
M81–234-4	17.3	57.5	409	165	51.0	86.5	235	165	19.3	26.8	87.9	26.8	65.4	2.54	2.44	16.7	2.27	
M81–234-4[a]	17.4	57.3	411	165	50.7	87.6	234	160.8	19.4	26.5	87.3	26.8	65.0	2.53	2.43	16.8	2.29	
M81–276-4	15.8	53.5	395	79.1	54.5	71.9	159	122	18.4	12.8	78.0	33.9	61.0	2.75	1.35	15.8	2.39	
M81–276-8	14.2	61.1	606	127	57.0	75.4	162	176	19.1	9.42	93.6	28.1	58.9	3.77	0.964	31.9	2.57	
Beata Ridge enriched																		
M81–217-7	88.6	35.0	228	904	39.1	333	84.6	107	12.6	9.18	166	15.4	78.4	14.05	0.977	97.2	13.5	
M81–229-9	59.5	38.0	367	852	51.7	269	135	217	18.4	15.8	339	20.3	159	41.35	1.02	185	27.4	
M81–229-12	49.4	38.0	346	730	44.9	220	96.1	119	18.6	12.6	412	21.3	164	42.6	0.646	173	28.4	
M81–229-12[a]	49.3	37.8	346	732	45.2	220	95.1	115	18.6	12.6	414	21.4	163	42.5	0.646	175	28.5	
M81–229-15	60.8	38.4	336	2015	64.0	629	100	98.0	15.0	10.1	167	16.5	81.9	20.75	0.416	74.5	14.3	
Beata Ridge LIP-like																		
M81–217-1	9.31	1.50	7.84	2.68	1.02	3.52	0.636	4.24	0.900	2.53	0.392	2.56	0.382	1.76	0.253	1.62	0.371	0.164
M81–217-2	7.96	1.29	6.79	2.41	0.837	3.09	0.565	3.76	0.799	2.25	0.348	2.27	0.340	1.54	0.226	0.857	0.317	0.113
M81–217-3	8.61	1.38	7.32	2.51	0.963	3.30	0.606	4.04	0.858	2.41	0.371	2.42	0.362	1.62	0.231	0.911	0.319	0.116
M81–217-4	8.20	1.34	7.21	2.56	0.987	3.32	0.611	4.05	0.862	2.41	0.368	2.41	0.358	1.62	0.235	0.595	0.262	0.120
M81–217-4[a]	8.21	1.34	7.26	2.55	0.989	3.30	0.610	4.08	0.870	2.44	0.370	2.43	0.358	1.63	0.237	0.614	0.264	0.119
M81–217-5	7.85	1.28	6.90	2.43	0.942	3.08	0.566	3.69	0.772	2.13	0.325	2.07	0.302	1.57	0.225	0.413	0.258	0.152
M81–217-6	9.21	1.49	7.93	2.76	1.06	3.59	0.651	4.29	0.896	2.51	0.383	2.49	0.364	1.81	0.256	0.507	0.301	0.163
M81–217-8	9.13	1.49	7.99	2.76	1.07	3.49	0.640	4.23	0.886	2.46	0.382	2.46	0.361	1.82	0.264	0.277	0.297	0.337
M81–217-9	8.00	1.33	7.03	2.46	0.946	3.18	0.585	3.86	0.810	2.27	0.348	2.25	0.327	1.64	0.231	0.248	0.268	0.348
M81–217-10	9.72	1.58	8.42	2.91	1.10	3.72	0.687	4.55	0.956	2.65	0.407	2.69	0.393	1.99	0.274	0.420	0.312	0.288
M81–217-11	8.92	1.45	7.66	2.70	0.96	3.50	0.640	4.27	0.910	2.55	0.393	2.57	0.383	1.73	0.241	0.881	0.269	0.211
M81–217-12	9.34	1.51	8.00	2.76	1.02	3.63	0.658	4.38	0.923	2.58	0.393	2.59	0.381	1.89	0.262	0.238	0.299	0.262
M81–217-13	10.7	1.75	9.28	3.18	1.16	4.08	0.755	5.03	1.07	3.01	0.466	3.04	0.454	2.11	0.311	0.777	0.347	1.01
M81–223-1	7.01	1.12	5.92	2.00	0.791	2.55	0.454	2.93	0.618	1.68	0.254	1.59	0.232	1.14	0.161	0.283	0.236	0.102
M81–223-1[a]	6.96	1.11	5.85	1.97	0.779	2.50	0.446	2.88	0.601	1.65	0.250	1.57	0.228	1.15	0.157	0.287	0.220	0.103
M81–223-2	5.23	0.847	4.49	1.59	0.668	2.04	0.373	2.43	0.518	1.45	0.226	1.45	0.218	1.05	0.150	0.214	0.173	0.181
M81–223-3	13.1	2.03	10.5	3.46	1.27	4.37	0.810	5.34	1.13	3.19	0.493	3.20	0.477	2.36	0.343	0.538	0.527	0.916
M81–223-5	12.2	1.95	10.1	3.44	1.27	4.25	0.778	5.13	1.05	2.90	0.443	2.88	0.419	2.50	0.412	0.723	0.367	1.89
M81–223-6	14.0	2.14	11.1	3.70	1.37	4.60	0.834	5.48	1.13	3.12	0.480	3.13	0.452	3.22	0.527	0.659	0.490	1.34
M81–223-7	8.51	1.37	7.40	2.57	0.971	3.39	0.618	4.05	0.859	2.38	0.363	2.35	0.347	1.60	0.235	0.249	0.256	0.563
M81–223-13	23.3	3.67	18.5	5.58	1.96	6.39	1.06	6.49	1.27	3.32	0.472	2.93	0.413	3.76	0.665	0.897	0.786	0.530

Please cite this article as: A. Dürkefälden, K. Hoernle, F. Hauff, et al., Age and geochemistry of the Beata Ridge: Primary formation during the main phase (~89Ma) of the Cari..., Lithos, https://doi.org/10.1016/j.lithos.2018.12.021

Table 3 (*continued*)

Sample	Li	Sc	V	Cr	Co	Ni	Cu	Zn	Ga	Rb	Sr	Y	Zr	Nb	Cs	Ba	La	
M81–229-2	8.89	1.40	7.46	2.60	0.990	3.26	0.594	3.82	0.789	2.14	0.328	2.06	0.301	0.994	0.262	0.622	0.266	0.150
M81–229-3	5.23	0.765	3.92	1.38	0.472	1.80	0.327	2.13	0.450	1.25	0.196	1.22	0.184	0.921	0.167	0.522	0.243	1.20
M81–229-4	4.73	0.714	3.70	1.35	0.423	1.76	0.323	2.14	0.458	1.27	0.204	1.31	0.195	0.868	0.154	0.395	0.229	0.462
M81–229-5	6.67	1.05	5.31	1.79	0.706	2.21	0.396	2.54	0.529	1.43	0.218	1.36	0.192	1.22	0.216	0.557	0.336	0.786
M81–229-13	9.18	1.59	7.63	2.32	0.767	2.85	0.503	3.26	0.684	1.89	0.291	1.85	0.274	1.47	0.285	0.437	0.437	0.608
M81–229-16	13.0	1.70	7.42	2.05	0.677	2.46	0.446	2.94	0.636	1.80	0.279	1.81	0.275	1.31	0.505	0.999	0.684	0.227
M81–229-19	9.09	1.50	8.20	3.03	1.16	4.24	0.803	5.55	1.20	3.38	0.515	3.30	0.470	2.13	0.256	0.365	0.319	0.218
M81–234-1	6.97	1.18	6.38	2.25	0.786	2.93	0.535	3.53	0.739	2.03	0.310	1.94	0.281	0.751	0.168	0.633	0.276	0.219
M81–234-6	8.02	1.31	6.97	2.49	0.987	3.18	0.582	3.80	0.798	2.19	0.331	2.13	0.312	1.53	0.227	0.712	0.248	0.778
M81–277-3	9.00	1.65	8.64	2.87	1.08	3.71	0.663	4.38	0.924	2.56	0.387	2.49	0.365	1.78	0.266	0.466	0.294	0.197
M81–279-1	15.3	2.43	12.6	4.27	1.59	5.70	1.08	7.41	1.61	4.64	0.711	4.64	0.672	4.11	0.425	0.347	0.687	1.39
M81–281-1	9.01	1.45	7.68	2.65	1.01	3.37	0.610	4.01	0.843	2.32	0.356	2.26	0.333	1.71	0.259	0.443	0.321	0.241
M81–283–4	10.1	1.65	8.83	3.13	1.18	4.13	0.762	5.10	1.08	3.03	0.460	2.99	0.435	2.10	0.283	0.747	0.349	0.229
M81–283-7	10.0	1.64	8.82	2.99	1.12	3.89	0.690	4.60	0.963	2.64	0.391	2.53	0.374	1.98	0.262	0.356	0.277	0.438
Beata Ridge depleted																		
M81–229-1	6.57	1.17	6.63	2.57	0.961	3.74	0.712	4.96	1.09	3.13	0.488	3.19	0.477	1.38	0.179	0.219	0.164	0.255
M81–229-14	2.48	0.412	2.35	0.983	0.466	1.50	0.288	1.99	0.433	1.20	0.178	1.13	0.172	0.615	0.055	0.460	0.080	0.238
M81–229-14[a]	2.49	0.415	2.36	0.982	0.466	1.49	0.287	1.99	0.431	1.21	0.179	1.13	0.168	0.617	0.052	0.455	0.077	0.238
M81–229-17	4.92	1.25	5.47	2.10	0.844	3.13	0.590	4.12	0.900	2.55	0.392	2.57	0.393	1.35	0.086	0.787	0.137	0.097
M81–234-4	6.86	1.16	6.67	2.69	1.08	3.78	0.723	4.96	1.07	3.04	0.472	3.08	0.451	1.90	0.180	0.269	0.220	0.227
M81–234-4[a]	6.94	1.18	6.78	2.67	1.07	3.78	0.720	5.00	1.08	3.05	0.474	3.09	0.453	1.88	0.176	0.252	0.218	0.223
M81–276-4	6.61	1.16	6.76	2.87	1.10	4.26	0.832	5.77	1.28	3.64	0.573	3.77	0.560	1.80	0.198	0.484	0.235	0.102
M81–276-8	6.92	1.13	6.49	2.68	1.07	3.91	0.749	5.17	1.12	3.18	0.489	3.20	0.463	1.79	0.234	0.288	0.261	0.382
Beata Ridge enriched																		
M81–217-7	29.6	3.94	16.8	3.64	1.17	3.46	0.534	3.12	0.607	1.63	0.244	1.53	0.228	1.90	0.731	0.396	1.09	0.346
M81–229-9	55.9	6.79	26.6	5.33	1.62	4.98	0.749	4.25	0.807	2.08	0.294	1.80	0.260	3.88	2.31	1.99	2.55	0.711
M81–229-12	59.0	7.02	27.3	5.45	1.74	5.05	0.780	4.39	0.839	2.20	0.315	1.96	0.286	3.87	2.34	1.66	2.68	0.652
M81–229-12[a]	59.4	7.06	27.7	5.53	1.75	5.08	0.792	4.43	0.847	2.21	0.319	1.98	0.286	3.88	2.37	1.68	2.70	0.657
M81–229-15	29.0	6.01	15.5	3.43	1.11	3.67	0.571	3.43	0.674	1.79	0.263	1.64	0.239	2.12	1.23	1.02	1.45	1.05

[a] Trace element replicate analysis on separate sample dissolution.

The geochemical distinction between the three groups, ranging from N-MORB to OIB, is clearly seen on Nb/Yb versus Th/Yb and TiO_2/Yb diagrams (Pearce, 2008; Fig. 7a-b), and the LIP-like samples cluster between the N-MORB and *E*-MORB compositions. Using the Zr/Y versus Nb/Y diagram of Fitton et al. (1997), almost all samples plot above the lower boundary of the Icelandic Plume Array with positive ΔNb (0.01–0.5) consistent with a plume source (Fig. 8). The LIP-like samples mainly cluster above the MORB field. In contrast, the enriched samples are shifted to higher Zr/Y and Nb/Y ratios, whereas the depleted samples have lower ratios and two depleted samples plot slightly below the Iceland Array (ΔNb = −0.03 and − 0.14).

3.4.2. Radiogenic isotopes

Initial $^{143}Nd/^{144}Nd$ and $^{176}Hf/^{177}Hf$ ratios range from 0.51281 to 0.51300 ($\varepsilon Nd_i = 5.47–9.34$) and from 0.28303 to 0.28317 ($\varepsilon Hf_i = 11.19–15.86$), respectively (Table 4). The data mainly cluster at intermediate values and belong to the samples identified as LIP-like based on trace element data (Fig. 9a-b). A second group with less radiogenic values corresponds to the trace element enriched (OIB-like) samples, while the trace element depleted (N-MORB-like) group displays more radiogenic Nd—Hf values. Some of the LIP-like samples overlap isotopically with the depleted group.

Whereas Nd and Hf isotope ratios are assumed to be largely insensitive to alteration processes ($R^2 = 0.81$ excluding the outlier of the LIP-like group; Fig. 9a) and can be used to geochemically characterize our samples, the Sr and Pb isotopic systems of our samples have been affected by seawater and hydrothermal alteration processes. On the initial $^{87}Sr/^{86}Sr$ versus $^{143}Nd/^{144}Nd$ diagram, the three distinct geochemical groups can be identified, but a number of samples are shifted to higher $^{87}Sr/^{86}Sr$ ratios due to seawater alteration (Appendix C, Fig. C.1). Thus we additionally performed Sr isotope analyses on strongly acid-leached powders in an attempt to remove surface alteration effects. In most cases, but not always, the strong leaching yielded the least radiogenic Sr isotope ratios.

Another possibility to get magmatic Sr isotopic composition is to measure Sr isotopes in plagioclase separates, since plagioclase preferably incorporates Sr and is often less altered than the whole rock matrix. We analyzed fresh plagioclase separates from the depleted group and found that the plagioclase Sr isotope ratios are indeed slightly lower than those in the whole rock (Table 4). To calculate initial ratios, we used the partition coefficients (Kd) of 0.1 for Rb and of 2 for Sr in plagioclase (Geochemical Earth Reference Model (GERM) partition coefficient (Kd) database) to estimate the Rb and Sr concentrations of the plagioclase. The Sr isotope ratios of the plagioclases form a more linear array on the initial Sr versus Nd isotope diagram (Appendix C, Fig. C.1). However, they are still shifted to higher $^{87}Sr/^{86}Sr$ isotope ratios than expected from Nd isotope ratios indicating seawater alteration.

The Pb isotopic system also appears to be largely disturbed in our sample suite. Initial $^{206}Pb/^{204}Pb$ versus $^{208}Pb/^{204}Pb$ and $^{207}Pb/^{204}Pb$ diagrams (Appendix C, Fig. C.2a-b) show that a number of samples do not lie on an expected array between depleted and enriched compositions, as is the case for example for data from the LNR (Dürkefälden et al., revised) and for the CLIP overall (Hauff et al., 2000a), but instead are under- or overcorrected. Such samples are shifted to the left and right of the mixing arrays in the thorogenic and uranogenic Pb isotope diagrams respectively (Appendix C, Fig. C2a-b). Due to open system behavior of U and Pb, affecting the parent/daughter ratios of the samples, and the much greater abundance of ^{238}U compared to ^{235}U, the $^{206}Pb/^{204}Pb$ ratio is generally most affected. Many of the samples display extremely high μ ($^{238}U/^{204}Pb$) values of 55–275 reflecting substantial U gain and/or Pb loss. Unfortunately, it is impossible to constrain when changes in U/Pb took place through alteration and if multiple changes of U/Pb took place throughout the history of the rock. Pb mobilization occurs during hydrothermal alteration, when the crust was still hot shortly after formation. As demonstrated on the Pb versus Ce/Pb diagram (Appendix C, Fig. C.3a), many of the samples have gained Pb, which could also affect its isotopic composition. The U versus Nb/U diagram (Appendix C, Fig. C.3b) shows that U was also added to most of the samples, which is common during low-temperature seawater alteration. Disturbance

Please cite this article as: A. Dürkefälden, K. Hoernle, F. Hauff, et al., Age and geochemistry of the Beata Ridge: Primary formation during the main phase (~89Ma) of the Cari..., Lithos, https://doi.org/10.1016/j.lithos.2018.12.021

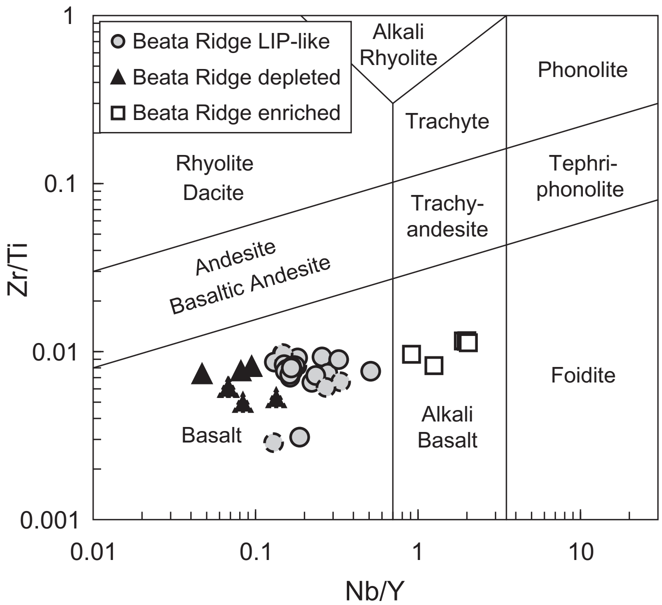

Fig. 4. Nb/Y versus Zr/Ti discrimination diagram after Pearce (1996). The majority of the samples plot within the basalt field but four samples plot within the field for alkali basalts. No evolved rocks plotting outside these two basaltic fields were sampled. Dashed symbol lines indicate gabbroic and doleritic samples.

of the U/Pb system is most obvious in the depleted sample group, since these samples do not display unradiogenic initial Pb isotope values as expected from the Nd—Hf isotope results. They are instead shifted to significantly higher Pb isotope ratios and plot in the vicinity of the more enriched samples (Appendix C, Fig. C.2a-b), indicating a complex disturbance history of the Pb isotope system that cannot be corrected.

In conclusion, Nd and Hf isotope ratios appear to represent undisturbed initial values in our sample suite and can be used without any restrictions. Sr isotope ratios are commonly affected by seawater alteration, and despite our attempt to get a primary Sr isotope signature by analyzing strongly leached powders and plagioclase separates, it was not possible to entirely remove the effects of seawater alteration. Since U addition is common during low-temperature alteration and Pb is mobilized by hydrothermal alteration, which appears to have been widespread in the Beata Ridge rocks, it was not possible to determine reasonable initial Pb isotope ratios for many of the samples.

4. Discussion

4.1. New evidence that much of the Beata Ridge was formed during the primary CLIP stage at ~89 Ma

Our new $^{40}Ar/^{39}Ar$ age dating results encompass a time span of about 15 Ma for the Beata Ridge ranging from 92.4 to 76.9 Ma, and the ages cover the main two stages of CLIP magmatism at ~89 Ma (95–83 Ma) and ~76 Ma (81–71 Ma; Hauff et al., 2000b; Hoernle et al., 2002, 2004; Sinton et al., 1998; Fig. 10). Thus far, the only comprehensive $^{40}Ar/^{39}Ar$ age dating at the Beata Ridge was conducted by Révillon et al. (2000b). They reported ages of ~81–55 Ma and thus documented the second magmatic CLIP phase and possibly a late, third magmatic episode, but they did not report any ages older than 81 Ma. In contrast, our new age data demonstrate that volcanic rocks belonging to the main CLIP event at ~95–83 Ma are clearly present at the Beata Ridge. Thus our results provide additional evidence that this CLIP stage represents a widespread event, including the central Caribbean. The only previously reported indication that the Beata Ridge basement formed during the initial CLIP stage comes from Site 151 on the southern Beata Ridge (Donnelly et al., 1973). Although dating of the drilled basaltic section was not possible, Santonian (86.3–83.6 Ma; www.stratigraphy.org)

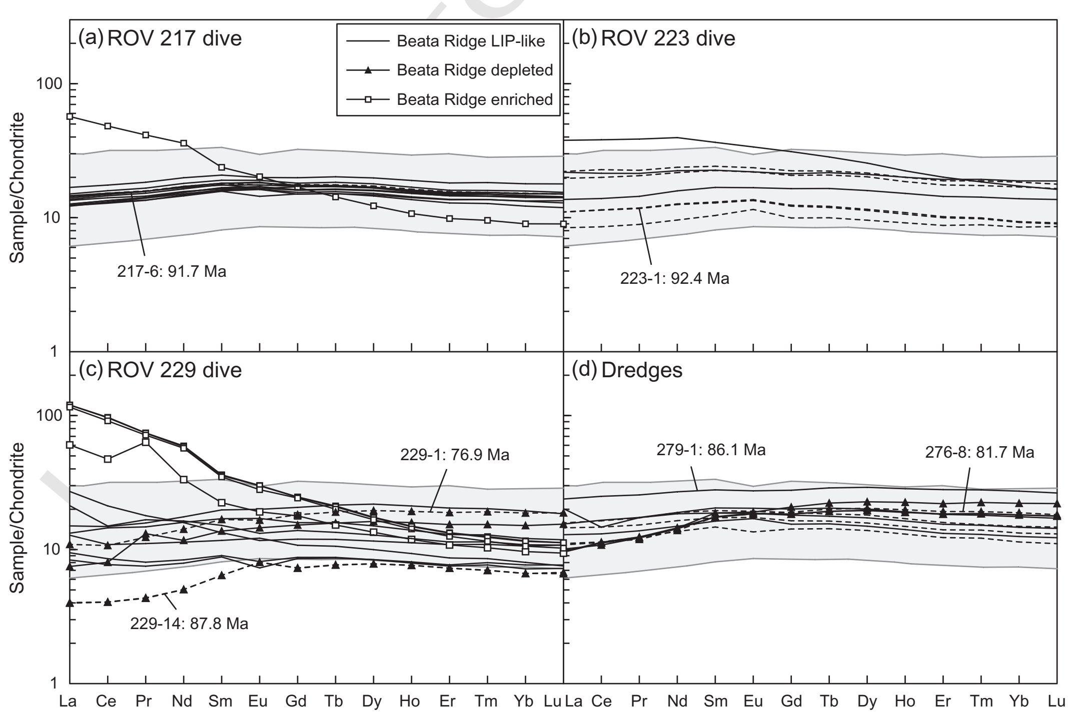

Fig. 5. (a)-(d) Rare earth element (REE) diagrams normalized to chondrite values after Sun and McDonough (1989) for samples from the Beata Ridge collected during three ROV dives and by dredging. Most of the samples show flat patterns, but a few samples have enriched (OIB-like) and some have more depleted (N-MORB-like) compositions. Rocks from the northern Beata Ridge (ROV 217 + 223) display largely uniform patterns, whereas samples from the central part (ROV 229) exhibit the largest geochemical variability. Most of the depleted compositions are found on the southern Beata Ridge (dredges). Dashed lines indicate gabbroic and doleritic samples. The gray shaded field shows common CLIP compositions (Hastie et al., 2008, 2016; Hauff et al., 2000a,b; Hoernle et al., 2004; Kerr et al., 1996b; Loewen et al., 2013; Révillon et al., 1999, 2000b; Sinton et al., 1998; White et al., 1999).

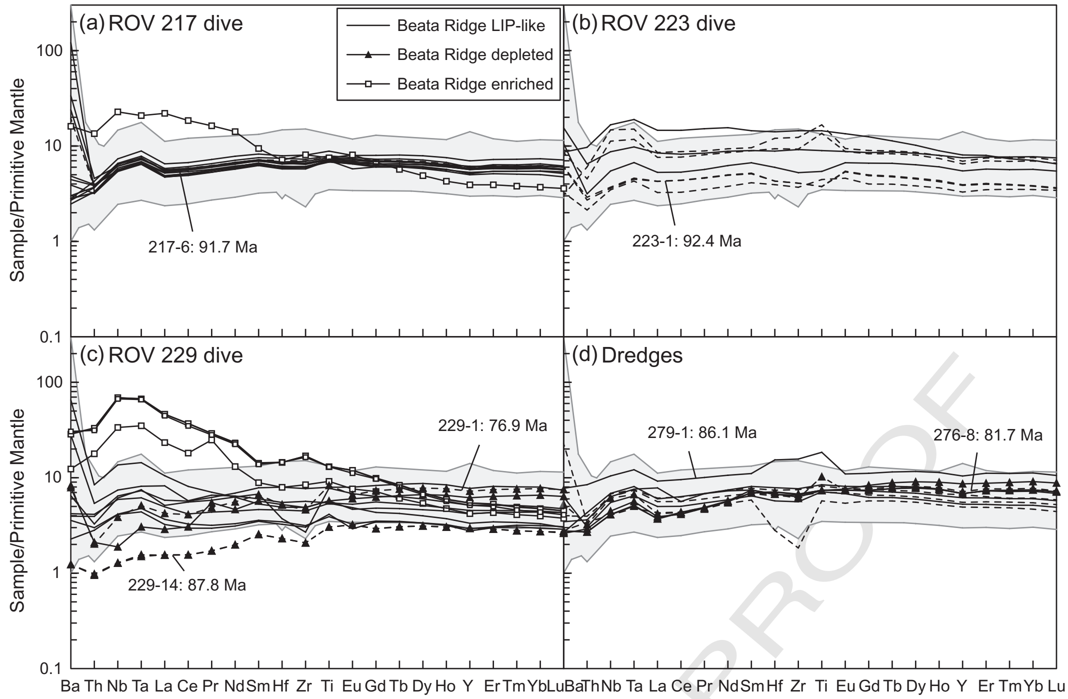

Fig. 6. (a)–(d) Multielement diagrams of largely immobile elements normalized to primitive mantle values after Hofmann (1988) for samples collected on the Beata Ridge confirming the observations made for the different REE patterns in Fig. 5.

sediments overlying the basalts provide a minimum age of ~84 Ma for the magmatic rocks.

Our dated samples were collected at different locations along the Beata Ridge indicating that the entire structure was formed during the main two CLIP stages. Our $^{40}Ar/^{39}Ar$ age dating, however, does not confirm the youngest intrusive rock ages (55–56 Ma) of Révillon et al. (2000b), which possibly represent minor late intrusive activity. If the two youngest ages from Révillon et al. (2000b) are excluded, the Beata Ridge formed primarily over a time interval of ~18 Ma (92–74 Ma). The Dumisseau Formation in southwestern Hispaniola is located very close to the Beata Ridge and represents an accreted fragment of the CLIP. Earlier studies revealed ages ranging from ~94–83 Ma and thus covering only the initial CLIP stage (Loewen et al., 2013; Sinton et al., 1998). A more recent study from Escuder-Viruete et al. (2016), however, shows that the Dumisseau Formation extends well into the second CLIP stage represented by a basalt dated at 74.2 ± 1.7 Ma and even covers a late phase represented by a 52.8 ± 1.7 Ma dolerite dike. Therefore the on-land results are comparable to those from the Beata Ridge confirming the suggestion of Escuder-Viruete et al. (2016) that the Beata Ridge may represent the continuation of this CLIP fragment in Hispaniola.

ROV 229 profile comprises two ages of 87.8 ± 5.9 Ma and 76.9 ± 2.7 Ma with the older age appearing to be stratigraphically above the younger age (Fig. 3c). Since both dated rocks are gabbros, their ages do not provide any stratigraphic information on the strata into which they intruded. The ROV diving revealed cliffs facing westwards which step eastwards with decreasing water depth. The morphology is interpreted to reflect step-faults, suggesting possible repetition of strata. Alternatively, the younger intrusion age at the base of profile 229 can be interpreted to belong to a later diking event.

4.2. A heterogeneous mantle source for the Beata Ridge and the CLIP containing depleted and enriched components

Our geochemical analyses show that the majority of the Beata Ridge samples are basaltic (Fig. 4) and have trace element characteristics, such as flat REE patterns (LIP-like group, Fig. 5), that are typical for global oceanic flood basalt provinces and are found throughout the CLIP in tholeiites of the main eruptive stage. On the Nb/Yb versus Th/Yb diagram (Pearce, 2008; Fig. 7a), the CLIP samples commonly cluster between N-MORB and E-MORB compositions within the MORB-OIB array. The narrow compositional range is attributed to the high degrees of melting and homogenization of the magma prior to eruption, as is, for example, also observed in many tholeiites from the Ontong-Java Plateau (Pearce, 2008). Our study, however, shows that the magmas erupted on the Beata Ridge are fairly heterogeneous on a local scale with a subset of samples displaying depleted (N-MORB-like) or enriched (OIB-like) compositions compared to the main LIP-like group lavas (Figs. 7-9). On the initial $^{143}Nd/^{144}Nd$ versus Th/Nd diagram, the data form linear arrays, implying two component mixing of mantle melts to form the intermediate LIP-like compositions (Fig. 9b).

Previous studies on the Beata Ridge by Révillon et al. (2000b) show that all sampled gabbros and dolerites display relatively flat REE patterns, whereas the only two basalts of their collection are geochemically enriched. Drilling at Site 151 on the southern part of the ridge also revealed basalts with enriched compositions (Geldmacher et al., 2003; Hauff et al., 2000a; Sinton et al., 1998; Thompson et al., 2004). Rocks from the nearby Dumisseau Formation in Hispaniola analyzed by Escuder-Viruete et al. (2016) can be divided into three groups based on TiO_2 contents and incompatible trace elements: low-Ti tholeiites (group I), high-Ti transitional basalts (group II) and high-Ti and LREE-enriched alkaline basalts (group III). Whereas group I overlaps with the common CLIP rocks, group II is more enriched and very similar to other rocks from the Dumisseau Formation studied by Loewen et al. (2013) and basalts from the Duarte Complex in Hispaniola (Escuder-Viruete et al., 2007; Lapierre et al., 1997, 1999), and is also similar to Site 151 basalts and the enriched Beata Ridge rocks from this study. Group III shows the most enriched compositions compared to rocks from the Beata Ridge and other Hispaniola samples ("Hispaniola enriched" in Figs. 7-8). Although no radiogenic isotope data are available for the three rock groups, the data suggest that the Dumisseau Formation lavas have similar chemical compositions to the Beata Ridge samples.

Please cite this article as: A. Dürkefälden, K. Hoernle, F. Hauff, et al., Age and geochemistry of the Beata Ridge: Primary formation during the main phase (~89Ma) of the Cari..., Lithos, https://doi.org/10.1016/j.lithos.2018.12.021

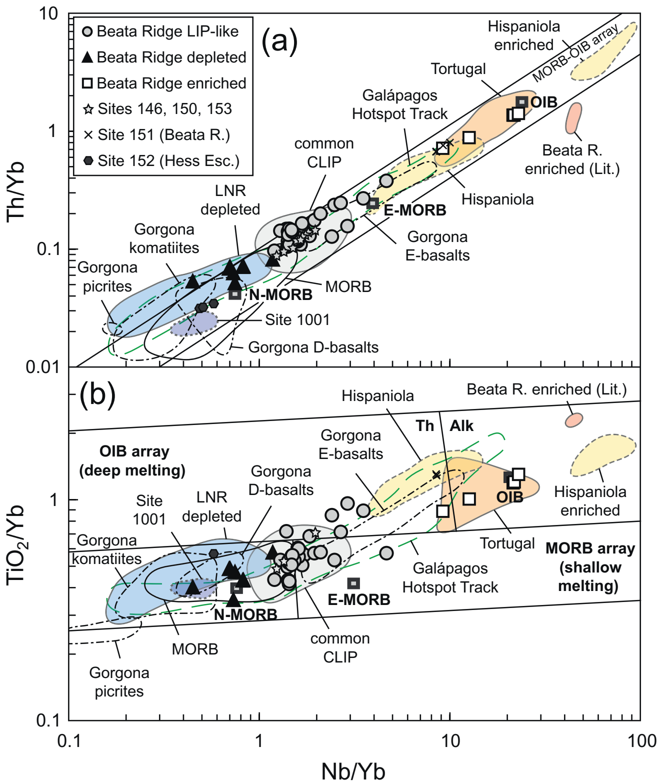

Fig. 7. Nb/Yb versus (a) Th/Yb and (b) TiO_2/Yb diagrams after Pearce (2008). The three different geochemical groups for the Beata Ridge can be distinguished, with depleted basaltic samples plotting in the area of N-MORB composition and enriched samples primarily in the area of alkalic OIB composition. LIP-like samples represent common CLIP compositions. Data from Sites 146 and 150–153 (Hauff et al., 2000a; Sinton et al., 1998) are additionally shown. Included are fields (solid, dashed and dotted lines) for common CLIP (data sources are in Fig. 4), Tortugal (Hauff et al., 2000b; Trela et al., 2017), Hispaniola (Escuder-Viruete et al., 2007, 2016; Lapierre et al., 1997, 1999; Loewen et al., 2013) and Hispaniola enriched (Dumisseau Formation, group III; Escuder-Viruete et al., 2016), enriched Beata Ridge basalts (labeled as "Beata R. enriched (Lit.)"; Révillon et al., 2000b), Site 1001 (Kerr et al., 2009), depleted samples from the Lower Nicaraguan Rise (LNR; Dürkefälden et al., revised), the Galápagos hotspot track (Buchs et al., 2016; Hauff et al., 2000a, 2000b; Hoernle et al., 2002; Trela et al., 2015), Gorgona komatiites, picrites, depleted (D-) and enriched (*E*-)basalts (Aitken and Echeverría, 1984; Arndt et al., 1997; Echeverría and Aitken, 1986; Kamenetsky et al., 2010; Kerr, 2005; Kerr et al., 1996a; Révillon et al., 2000a; Serrano et al., 2011) and MORB (PetDB at http://www.earthchem.org/petdb). Analytical errors are smaller than the symbol size.

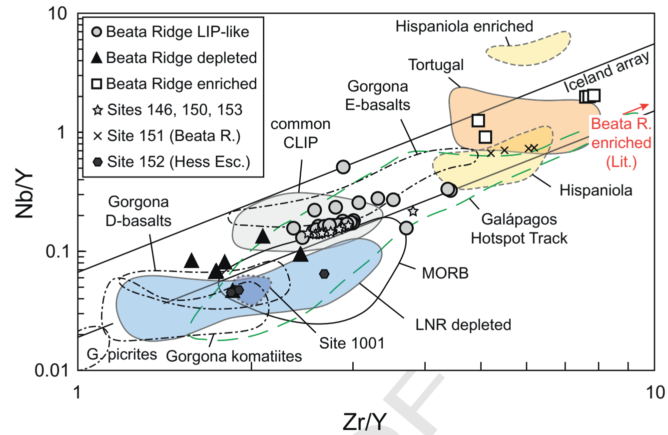

Fig. 8. Zr/Y versus Nb/Y diagram after Fitton et al. (1997). The samples from all three geochemical groups generally plot within the Iceland array with positive ΔNb values (ΔNb = deviation from the lower boundary of the Iceland array) indicating derivation from a plume-like mantle source, even for the most depleted compositions. The majority of the LIP-like samples cluster above the MORB field together with most of the common CLIP data. OIB-like samples plot at higher ratios, whereas the depleted samples have lower ratios. Analytical errors are smaller than the symbol size. Symbols and data sources are the same as in Figs. 5 and 7.

Rocks with depleted compositions have not been found thus far on the Beata Ridge nor in CLIP-related formations in Hispaniola. Our sampling of geochemically depleted rocks, however, clearly shows that a depleted component was also involved in the generation of some of the Beata Ridge rocks. The compositions are similar to those of depleted rocks found on the nearby LNR, including the Hess Escarpment (Dürkefälden et al., revised; Geldmacher et al., 2003; Hauff et al., 2000a; Kerr et al., 2009; Sinton et al., 1998; Thompson et al., 2004; Fig. 1b), although the samples from this study do not show the extreme depletion of the LNR rocks (Figs. 7-9). This similarity points to a common depleted source for the depleted magmas of both the Beata Ridge and LNR regions. On the Zr/Y versus Nb/Y diagram after Fitton et al. (1997), however, the depleted Beata Ridge samples plot within the Iceland (plume) array, whereas the depleted LNR samples plot below the array and partly within the MORB field. These observations indicate that the depleted Beata Ridge samples are primarily plume-derived and that the depleted LNR compositions reflect a mixture of plume and MORB material. Until now, depleted compositions in CLIP magmas have been observed only rarely except for komatiites, picrites and depleted (D-)basalts on Gorgona Island (Aitken and Echeverría, 1984; Arndt et al., 1997; Echeverría and Aitken, 1986; Kerr et al., 1996a; Révillon et al., 2000a; Serrano et al., 2011). The Site 1001 lavas (Kerr et al., 2009) serve as the depleted end member for the LNR (Dürkefälden et al., revised). Based on our new data from the Beata Ridge, it is likely that the highly depleted Site 1001 lavas also serve as the depleted end member for the entire central Caribbean region and possibly for the entire CLIP together with the Gorgona komatiites and picrites. We note, however, that on the εNd_i versus εHf_i diagram, several of our depleted samples show a rough trend toward Gorgona D-basalts, komatiites and picrites. This is consistent with the assumption of Dürkefälden et al. (revised) that the depleted plume component in the CLIP lavas may have slightly different flavors represented by LNR rocks and Gorgona komatiites and picrites. Additionally, the enriched component in the Beata Ridge samples could serve as the enriched end member for the CLIP together with rocks from the Tortugal region in Costa Rica (Hauff et al., 2000b; Trela et al., 2017) and from Hispaniola (Escuder-Viruete et al., 2007, 2016; Lapierre et al., 1997, 1999; Loewen et al., 2013; Fig. 9).

4.3. Processes leading to the heterogeneous compositions of the Beata Ridge

Our geochemical investigations show compositional differences for samples from the northern, central and southern part of the Beata Ridge. The compositions of the samples collected during ROV 217 and 223 dives on the northern part of the ridge are uniform over the entire profiles with relatively flat REE patterns and intermediate isotopic compositions. The only exception is sample 217–7 with an enriched pattern (Figs. 5a and 6a; Tables 3 and 4). Likewise, the two enriched basalts presented by Révillon et al. (2000b) were collected on the northern Beata Ridge. The ROV 229 profile on the central Beata Ridge reveals an entirely different signature. The depleted, LIP-like and enriched groups are present but do not correlate with stratigraphic position. The dredged rocks from the southern Beata Ridge have intermediate LIP-like and depleted geochemical compositions, but enriched compositions are absent. Site 151 rocks on the southern part, however, display enriched compositions (Geldmacher et al., 2003; Hauff et al., 2000a; Sinton et al., 1998; Thompson et al., 2004). Therefore LIP-like and enriched rocks are found throughout the Beata Ridge and depleted rocks only on the central and southern parts.

These observations imply that despite the large degrees of partial melting generally involved in the formation of flood basalts, the depleted and enriched components in the plume head were not effectively

Table 4
Sr-Nd-Pb-Hf isotope data from the Beata Ridge.

Sample	$^{87}Sr/^{86}Sr$[b]	±2σ	$^{87}Sr/^{86}Sr$[c]		±2σ	$^{87}Sr/^{86}Sr$[d]	±2σ	$^{87}Sr/^{86}Sr_i$	$^{143}Nd/^{144}Nd$	±2σ	εNd	$^{143}Nd/^{144}Nd_i$	$εNd_i$	
Beata Ridge LIP-like														
M81–217-6	0.703085	4	0.703113		6	0.703085	4	0.70253	0.513050	5	8.04	0.51292	7.79	
M81–217–9	0.703081	5	0.703309		6	0.703081	5	0.70273	0.513040	6	7.84	0.51292	7.69	
M81–223-1	0.703359	6	0.703359		6	0.703587	5	0.70327	0.513035	5	7.75	0.51291	7.57	
M81–223-2	0.703420	5	0.703420		5	0.703942	5	0.70332	0.513053	4	8.10	0.51293	7.92	
M81–223-3	0.703503	5	0.703592		6	0.703503	5	0.70345	0.513038	5	7.81	0.51293	7.78	
M81–223-7	0.703664	5	0.703664		5	0.703801	5	0.70339	0.513036	6	7.76	0.51292	7.63	
M81–223-13	0.703258	6	0.703511		6	0.703258	6	0.70330	0.513008	6	7.21	0.51290	7.27	
M81–229-4	0.703259	5	0.703436		4	0.703259	5	0.70282	0.513040	6	7.84	0.51292	7.60	
M81–229-16									0.512965	4	6.39	0.51287	6.72	
M81–229-19	0.703045	5	0.703170		6	0.703045	5	0.70257	0.513116	7	9.32	0.51299	9.04	
M81–234-1									0.513036	6	7.77	0.51292	7.60	
M81–234-1[a]									0.513028	5	7.60	0.51291	7.43	
M81–277-3	0.703259	6	0.703748		5	0.703259	6	0.70278	0.513010	6	7.25	0.51290	7.22	
M81–277-3[a]	0.703690	6	0.703690		6			0.70272	0.513021	3	7.48	0.51291	7.44	
M81–279-1	0.703925	5	0.706853		5	0.703925	5	0.70253	0.513078	4	8.59	0.51296	8.41	
M81–281-1	0.703189	5	0.703374		6	0.703189	5	0.70284	0.513029	6	7.62	0.51291	7.51	
M81–283–4	0.703022	5	0.703556		6	0.703022	5	0.70304	0.513043	5	7.90	0.51292	7.72	
Beata Ridge depleted														
M81–229-1	0.703546	5	0.703759		5	0.703546	5	0.70348	0.513094	3	8.89	0.51298	8.53	
M81–229-1	0.703463	4						0.70345						
Plag separates														
M81–229-14	0.703081	6	0.703081		6	0.703176	6	0.70277	0.513153	7	10.05	0.51300	9.34	
M81–229-14	0.702926	4						0.70291						
Plag separates														
M81–234-4	0.703170	4	0.703761		5	0.703170	4	0.70270	0.513126	4	9.52	0.51299	8.92	
M81–234-4	0.703069	4						0.70302						
Plag separates														
M81–276-4	0.703201	5	0.703800		6	0.703201	5	0.70323	0.513122	4	9.43	0.51298	8.80	
M81–276-4	0.703194	4						0.70317						
Plag separates														
M81–276-8	0.703239	5	0.703623		6	0.703239	5	0.70329	0.513110	5	9.21	0.51298	8.67	
M81–276-8	0.703200	5						0.70318						
Plag separates														
Beata Ridge enriched														
M81–217-7	0.703529	6	0.703529		6	0.703660	5	0.70334	0.512886	5	4.84	0.51281	5.47	
M81–229-9	0.703388	5	0.703388		5	0.703439	5	0.70323	0.512905	4	5.22	0.51283	5.95	
M81–229-9[a]	0.703399	6	0.703399		6	0.703439	5	0.70324	0.512906	4	5.23	0.51283	5.96	
M81–229-15	0.703471	6	0.703471		6	0.703880	5	0.70326	0.512914	6	5.39	0.51284	6.09	
Beata Ridge LIP-like														
M81–217-6	19.2009	13	15.5661	12	38.6917	35	18.90	15.55	38.51	0.283126	5	12.52	0.28307	12.80
M81–217–9	19.0916	6	15.5592	4	38.5968	12	17.90	15.50	38.30	0.283119	6	12.27	0.28307	12.54
M81–223-1	19.2374	18	15.5612	16	38.7464	41	18.90	15.55	38.49	0.283122	5	12.36	0.28307	12.62
M81–223-2	19.2949	4	15.5624	32	38.6824	8	18.57	15.53	38.46	0.283119	5	12.26	0.28307	12.47
M81–223-3	19.6953	8	15.6051	8	38.9388	25	18.23	15.54	38.66					
M81–223-7	21.8446	14	15.6853	12	39.0692	36	19.84	15.59	38.77	0.283125	6	12.48	0.28307	12.60
M81–223-13	19.4209	12	15.5800	10	38.8658	29	18.91	15.56	38.62					
M81–229-4	19.7303	14	15.6152	13	39.1615	33	18.72	15.57	39.00	0.283214	5	15.63	0.28316	15.70
M81–229-16	19.6215	15	15.6132	14	39.3106	43	19.42	15.60	39.12					
M81–229-19	19.3706	14	15.5771	12	38.7559	31	18.86	15.55	38.51	0.283178	6	14.34	0.28313	14.44
M81–234-1	19.5867	21	15.5885	16	38.7782	43	19.29	15.57	38.66	0.283161	8	13.74	0.28307	12.55
M81–234-1[a]	19.7410	12	15.5952	10	38.7903	3	19.44	15.58	38.67				0.28307	12.55

(continued on next page)

Table 4 (*continued*)

Sample	$^{87}Sr/^{86}Sr$[b]	±2σ	$^{87}Sr/^{86}Sr$[c]		±2σ	$^{87}Sr/^{86}Sr$[d]	±2σ	$^{87}Sr/^{86}Sr_i$	$^{143}Nd/^{144}Nd$	±2σ	εNd	$^{143}Nd/^{144}Nd_i$	$εNd_i$	
M81–277-3	19.3103	9	15.5745	8	38.7484	3	18.95	15.56	38.57	0.283114	5	12.09	0.28307	12.32
M81–277-3[a]	19.3148	19	15.5688	16	38.7224	39	18.95	15.55	38.55	0.283123	6	12.41	0.28307	12.64
M81–279-1	23.2176	19	15.7721	14	39.4318	36	19.52	15.60	38.83	0.283163	5	13.83	0.28312	14.41
M81–281-1	19.6097	13	15.5909	11	38.8875	3	19.14	15.57	38.68					
M81–283–4	19.2451	9	15.5956	9	38.7844	3	18.98	15.58	38.65	0.283125	5	12.47	0.28308	12.67
Beata Ridge depleted														
M81–229-1	20.4547	34	15.6226	27	39.5212	69	19.53	15.58	39.33	0.283198	5	15.07	0.28312	14.22
M81–229-14	20.2527	21	15.6558	18	38.9704	49	19.79	15.63	38.92	0.283202	6	15.21	0.28313	14.80
M81–234-4	19.8198	16	15.6020	13	38.8979	34	19.09	15.57	38.67	0.283198	5	15.08	0.28314	15.03
M81–276-4	19.2437	7	15.5793	6	38.8347	18	19.06	15.57	38.70	0.283226	6	16.04	0.28315	15.38
M81–276-8	20.1554	240	15.5698	185	38.9368	456	19.05	15.52	38.69	0.283226	7	16.07	0.28317	15.86
Beata Ridge enriched														
M81–217-7	20.4124	12	15.6384	10	39.7919	27	19.64	15.60	38.99	0.283073	7	10.63	0.28304	11.56
M81–229-9	20.0548	12	15.6497	14	39.6732	47	19.74	15.63	39.31	0.283050	4	9.82	0.28303	11.19
M81–229-9[a]	19.9697	12	15.6525	10	39.6193	29	19.66	15.64	39.25					
M81–229-15	19.8932	6	15.6207	6	39.4805	19	19.00	15.58	39.07	0.283079	5	10.84	0.28305	11.84

Inital isotope ratios were calculated using measured Sr-Nd-Hf-Pb isotope ratios from the sample dissolution of leached chips or powders.
±2σ internal errors are shown for the last significant digit(s).
[a] Isotope replicate analyses on separate sample dissolution.
[b] Least radiogenic $^{87}Sr/^{86}Sr$ from either leached chips or powder.
[c] Leached chips: 2 N HCl at 70 °C for 1 h and then triple rinsed in 18.2 MΩ H_2O.
[d] Leached powder: 6 N HCl at 150 °C for 48 h and then triple rinsed in 18.2 MΩ H_2O.

homogenized. Although in some regions of the CLIP, such as in the northern part of the Beata Ridge and in Costa Rica, Colombia and on Curaçao and Aruba, the uniform geochemical characteristics point to thorough mixing of the components, the sampled basement sequence of the central Beata Ridge (ROV 229 dive) clearly preserved the depleted and enriched source compositions, as well as mixed compositions (Figs. 5c and 6c). Thus it is possible that the plume head comprised variably-sized domains of the distinct enriched and depleted mantle source compositions and homogenized melt domains of intermediate LIP-like compositions, and that these different domains were variably sampled during the formation of the CLIP. These interpretations are also consistent with mantle plumes being composed of enriched blobs or streaks in a depleted refractory matrix (Hastie et al., 2016; Hoernle et al., 2000; Kerr et al., 1995, 2002b). As the different profiles on the Beata Ridge are only ~50–100 km apart and a high level of heterogeneity in samples collected along the ROV 229 profile is observed, these heterogeneities within the plume head evidently occur on a relatively small scale (<100 km). This is consistent with Kerr et al. (2002b) who also postulated small-scale heterogeneities within the plume beneath the CLIP with length scales of tens of kilometers or less, as demonstrated by lavas from the Central Cordillera (Colombia) and from Gorgona.

The Osa Igneous Complex exposed on the Osa Peninsula in Costa Rica comprises accreted seamounts assumed to be part of the early Galápagos hotspot track (Buchs et al., 2016). These rocks, as well as lavas from the Galápagos archipelago (Hoernle et al., 2000), show depleted and enriched geochemical compositions very similar to those from the CLIP rocks that have been interpreted to be derived from enriched and depleted components in the plume. They indicate that such geochemical heterogeneities are present during both the plume head and plume tail stage and suggest that they are an integral part of the plume source region.

4.4. Temporal geochemical evolution of the Beata Ridge

A comparison of age and geochemical compositions of our samples shows a rough trend from older LIP-like to younger more depleted samples (Fig. 11). While the oldest ~92–86 Ma samples mainly have common CLIP-like compositions, the ~82 Ma and ~77 Ma old gabbros (276–8 and 229–1) display depleted compositions. Likewise, 94–92 Ma old basalts from drill sites 146 and 150 in the Venezuelan Basin and two 90–88 Ma old rocks on Curaçao display LIP-like signatures, whereas a 75.8 ± 4.0 Ma diabase sill on Curaçao is depleted (Sinton et al., 1998). Furthermore, the ~81 Ma highly depleted Site 1001 basalts at the Hess Escarpment also belong to the second magmatic phase (Kerr et al., 2009; Sinton et al., 2000). Rocks with depleted compositions belonging to the main event have only been found on Gorgona thus far and there is some question if the Gorgona komatiites really belong to the CLIP event (Kerr, 2005; Kerr et al., 2002a). These observations suggest that the depleted source component was preferentially sampled during the later stage of CLIP volcanism (Sinton et al., 1998). We note, however, that LIP-like rocks were also erupted in the second CLIP stage on the Beata Ridge (Révillon et al., 2000b), Hispaniola (Escuder-Viruete et al., 2016), Curaçao (Loewen et al. (2013) and the LNR (Dürkefälden et al., revised). Enriched compositions are rare in the second stage of the CLIP thus far, indicating that these domains of the upwelling plume head have been largely exhausted during the first stage of melting. On the other hand, depleted magmas are more abundant during the second CLIP stage, suggesting re-melting of residual plume material and enhanced melting of depleted upper mantle MORB-source material.

Reviewing the age and geochemical data, we propose that a large portion of the Beata Ridge was formed by extrusive activity during the main CLIP stage at ~89 Ma (Fig. 12a). We sampled abundant extrusive rocks throughout the structure, such as pillow and sheet lavas, pillow breccias and volcaniclastic rocks, and two of the dated samples representing the main event are basaltic rocks. Furthermore, tuffs with

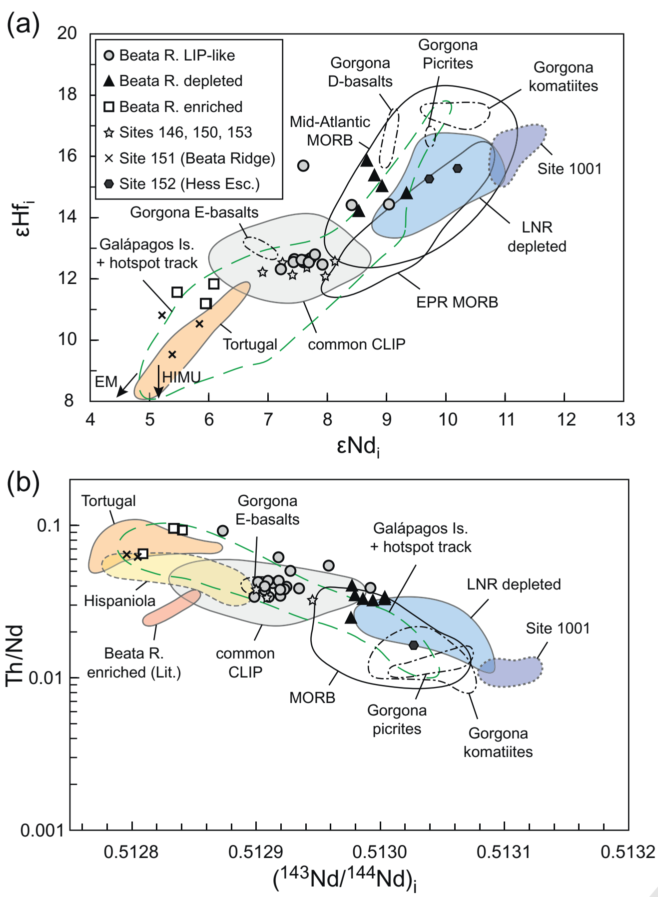

Fig. 9. (a) Initial εNd versus εHf diagram showing the three groups of the Beata Ridge samples: Depleted, LIP-like and enriched. Also included are data from Sites 146 and 150–153 (Geldmacher et al., 2003; Hauff et al., 2000a; Thompson et al., 2004). Fields are shown for common CLIP (Geldmacher et al., 2003; Hastie et al., 2008, 2016; Hauff et al., 2000a, 2000b; Thompson et al., 2004; White et al., 1999), Tortugal (Trela et al., 2017), Site 1001 (Kerr et al., 2009), depleted samples from the Lower Nicaraguan Rise (LNR; Dürkefälden et al., revised), Gorgona (Thompson et al., 2004), Galápagos Islands (Is.; GEOROC at http://georoc.mpch.gwdg.de/georoc/) and hotspot track (Geldmacher et al., 2003; Hauff et al., 2000b) and Mid-Atlantic and East Pacific Rise (EPR) MORB (PetDB at http://www.earthchem.org/petdb). (b) Initial ^{143}Nd/^{144}Nd versus Th/Nd diagram. The data form rough linear arrays extending from enriched to depleted compositions with most of the samples, showing LIP-like compositions, which cluster between the enriched and depleted groups. Data sources are the same as in Figs. 5, 7 and 9a. Analytical errors are smaller than the symbol size. Initial isotopic compositions are calculated using an age of 85 Ma and the calculation is described in Appendix C.

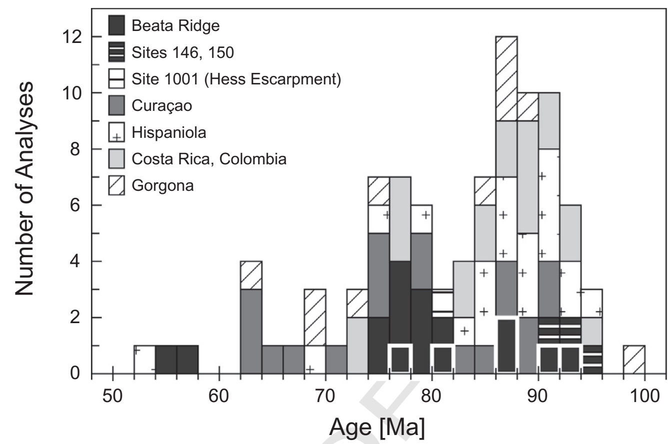

Fig. 10. Histogram of ^{40}Ar/^{39}Ar age data from the CLIP: published and from this study. Two magmatic events (one at ~95–83 Ma and the other at ~81–71 Ma; Hoernle et al., 2002, 2004) can be clearly distinguished with scattered ages from 72 to 52 Ma. Besides the age data from this study (outlined with white boxes), published data from the Beata Ridge and from Sites 146 and 150, Site 1001, Curaçao, Hispaniola, Costa Rica, Colombia and Gorgona are also shown (Alvarado et al., 1997; Escuder-Viruete et al., 2007, 2011, 2016; Hauff et al., 2000b; Kerr et al., 1997, 2002a; Lapierre et al., 1999; Loewen et al., 2013; Révillon et al., 2000b; Serrano et al., 2011; Sinton et al., 1997, 1998, 2000).

accretionary lapilli were collected during two of the ROV dives (Figs. 2 and 3). Since accretionary lapilli form in a subaerial environment during explosive volcanic eruptions in the eruptive column, they indicate that there was also some subaerial volcanic activity during the early formation of the Beata Ridge and that the ridge must have subsided afterwards. Accretionary lapilli are deposited subaerially or subaqueously in relative proximity to the volcano. The lapilli in our samples are surrounded by a very fine-grained matrix and thus deposition is assumed to have occurred subaerially, since subaqueous deposition would result in separation of the lapilli from the finest material (Werner et al., 2011). The occurrence of accretionary lapilli tuffs with an oceanic plateau geochemical signature in other rock formations belonging to the CLIP, namely the Aruba Lava Formation (White et al., 1999; Wright and Wyld, 2011) and the western Cordillera in Colombia (Buchs et al., 2018), supports the assumption that parts of the CLIP formed under subaerial conditions and that this may have also been the case for at least parts of the Beata Ridge.

We believe that the first stage at ~89 Ma was related to a major pulse of (the Galápagos?) mantle plume (or plume head), and that the enriched component together with a mixture of the enriched and the depleted components to form LIP-like compositions was preferably sampled during this stage. The second stage at ~76 Ma probably represents further melting or remelting of residual plume material and upper mantle, since the Caribbean had drifted away from the plume stem, located under Central America at that time. Magmas associated with the second stage appear to have been primarily intrusive at the Beata Ridge (Fig. 12b), represented by the ~82 and ~77 Ma old gabbros from this study and the gabbros and dolerites (~81–74 Ma) analyzed by Révillon et al. (2000b). During this stage, depleted compositions became more pronounced. Residual plume material, which consisted of a larger portion of the depleted component after melting and melt extraction of the more enriched material, remained in the upper mantle. This still hot, residual plume material and depleted upper mantle upwelled, possibly due to lithospheric thinning as a result of extensional processes that also formed the Beata horst block and adjacent Haiti subbasin, and melted by decompression (Dürkefälden et al., revised; Kerr et al., 2009; Sinton et al., 2000). The geochemical data, however, indicate that enough enriched plume material remained to generate melts that could be mixed with depleted melts (or that enough mixed plume material remained that melted), leading to the contemporaneous generation of LIP-like melts on the Beata Ridge.

Our observations, indicating that the early rocks on the Beata Ridge probably formed as a result of primarily extrusive magmatic activity, are in contrast to the hypothesis of Révillon et al. (2000b) that a large part of the ridge may represent an imbricated sill/dike complex based on their almost exclusive sampling of gabbros and dolerites. Our observations also differ from the suggestion of Mauffret and Leroy (1997) and Mauffret et al. (2001) that the extrusive layer on the Beata Ridge may be very thin. On the other hand, our results are in agreement with the onland studies of the nearby Dumisseau Formation in Hispaniola, where sampling of abundant volcanic rocks likewise points to extensive extrusive activity (Escuder-Viruete et al., 2016;Loewen et al., 2013 ; Sinton et al., 1998). The ages and rock types of the study by Révillon et al. (2000b) indicate that they mainly sampled the second magmatic phase, which may represent a primarily intrusive event at the Beata Ridge.

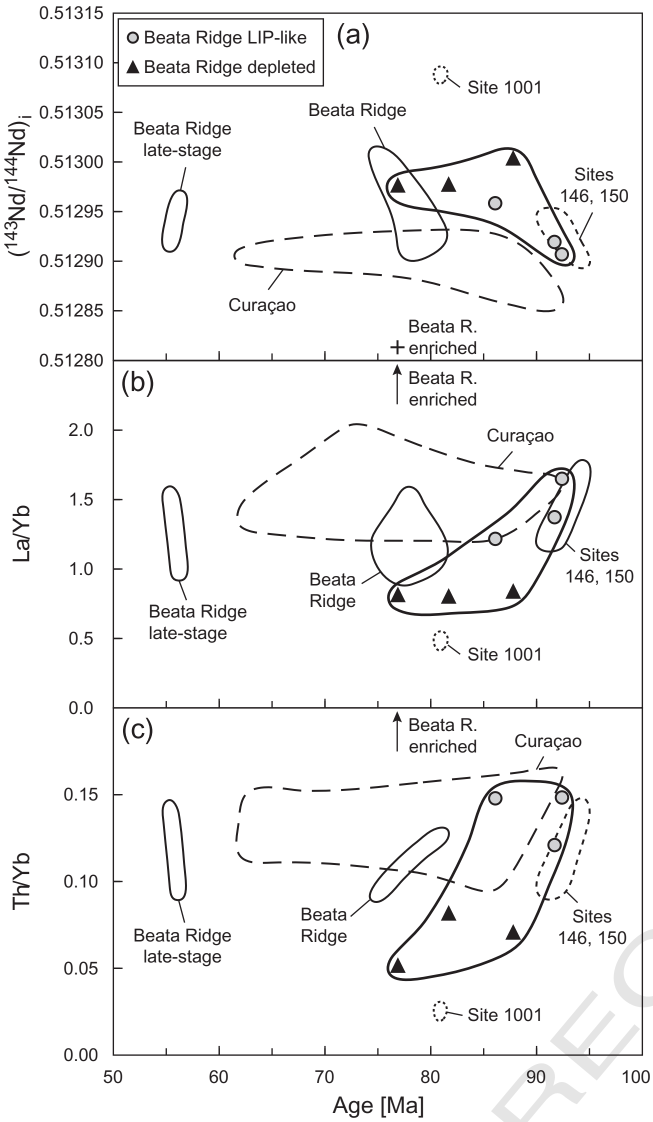

Fig. 11. Age versus (a) initial $^{143}Nd/^{144}Nd$, (b) La/Yb and (c) Th/Yb diagrams. Our new $^{40}Ar/^{39}Ar$ age data show a rough trend from older samples with more LIP-like compositions to younger samples with more depleted compositions. Data from Site 1001 extend this trend to more depleted compositions (; Kerr et al., 2009; Sinton et al., 2000), and geochemical compositions from Sites 146 and 150 in the Venezuelan Basin (dotted line fields; Sinton et al., 1998) are similar to those from this study for the same age range. The ages for the Beata Ridge, however, determined by Révillon et al. (2000b) (solid black line fields and cross/arrow for the enriched basalt) and for Curaçao (dashed line field; Loewen et al., 2013) do not follow this trend.

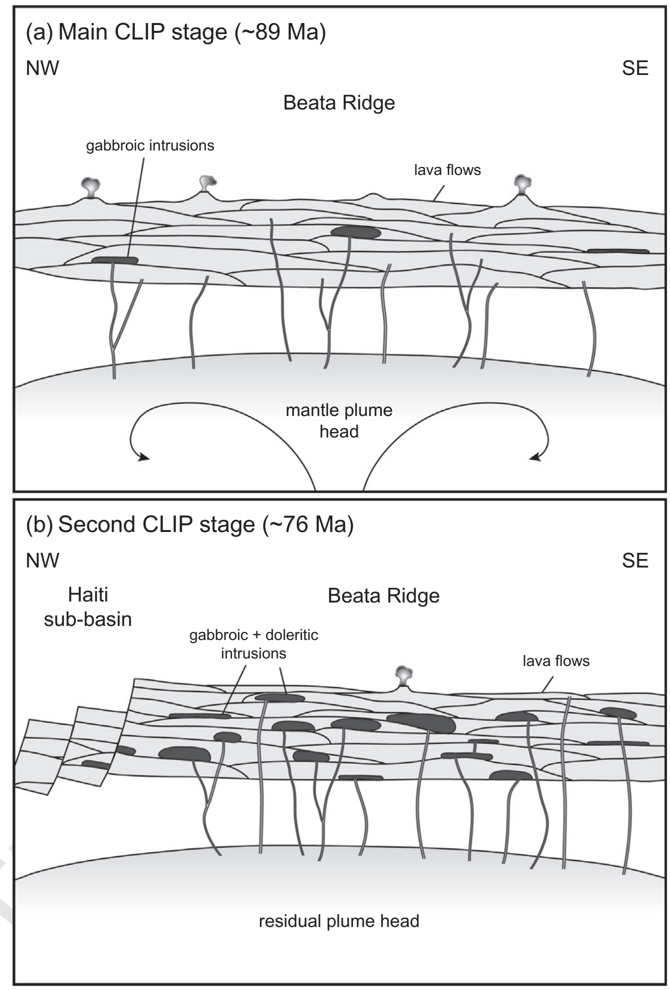

Fig. 12. Cartoon showing the Beata Ridge (a) during the main CLIP stage at ~89 Ma and (b) during the second CLIP stage at ~76 Ma. The main stage is assumed to be characterized by mainly extrusive magmatic activity, whereas the second stage was probably a largely intrusive event.

4.5. Comparison of the CLIP with other LIPs

Earlier investigations suggested that LIPs are emplaced in geologically short periods of time of only ~2–3 Ma during large-scale catastrophic events (e.g., Courtillot and Renne, 2003; Duncan and Pyle, 1988). However, this was mainly based on data from continental flood basalt provinces, and the increasing investigation of oceanic LIPs in particular shows that LIPs were often formed over longer time scales and during two or more magmatic episodes of different durations. This is observed for the CLIP with a time span of ~30 Ma and at least two major magmatic phases (Fig. 10), which is further confirmed by our study, but is also observed for other oceanic LIPs such as the Ontong Java Plateau (~125–119 Ma and ~94–86 Ma; Tejada et al., 2002 and references therein), Manihiki Plateau (>125 Ma, ~125–116 Ma and ~100–65 Ma; Hoernle et al., 2010; Pietsch and Uenzelmann-Neben, 2015; Timm et al., 2011), the Kerguelen Plateau/Broken Ridge (~120–95 Ma; Coffin et al., 2002; Duncan, 2002) and Shatsky Rise (~145–134 Ma and ~129 Ma; Geldmacher et al., 2014; Tejada et al., 2016).

Regarding the geochemical composition, oceanic LIP rocks typically display a narrow compositional range with relatively flat chondrite-normalized REE patterns and intermediate radiogenic isotope ratios, also represented by the bulk of the CLIP rocks. It is, however, increasingly shown that other oceanic LIPs are also geochemically more heterogeneous than previously assumed displaying involvement of enriched and depleted components. For example, two enriched components are found on the Ontong Java Plateau (Kroenke/Kwaimbaita and Singgalo groups; e.g., Tejada et al., 2002) and a depleted component has been proposed based on studies of melt inclusions in olivines of an Ontong Java basalt (Jackson et al., 2015). At the Manihiki Plateau enriched high-Ti group lavas have been identified (e.g., Golowin et al., 2018; Hoernle et al., 2010; Timm et al., 2011). Low-Ti basalts from Manihiki require both a depleted and enriched component to explain their U-shaped incompatible element patterns and isotopic compositions (Golowin et al., 2017a, 2017b; Timm et al., 2011). At the Shatsky Rise both enriched (high-Nb type lavas) and depleted (U1349 type lavas) components have been identified (e.g., Heydolph et al., 2014 and references therein). Kerguelen Plateau/Broken Ridge rocks display a wide range in geochemical compositions, but they are likely contaminated by a continental component (e.g., Mahoney et al., 1995). Thus the widespread occurrence of LIP rocks with a narrow compositional range seems to reflect effect mixing of at least two geochemically distinct mantle source components rather than derivation from a homogeneous mantle source.

5. Conclusions

Our new $^{40}Ar/^{39}Ar$ age data combined with published data (Révillon et al., 2000b) from the submarine Beata Ridge, which represents a part of the Caribbean Large Igneous province (CLIP), show that magmatic activity in the Central Caribbean lasted at least 18 Ma, from ~92 to ~74 Ma, supporting the assumption of long-term volcanism for the CLIP. We cannot, however, confirm the young $^{40}Ar/^{39}Ar$ ages of 55–56 Ma from Révillon et al. (2000b). Our combined geochemical data reveal for the first time depleted compositions in igneous samples from the Beata Ridge besides common LIP-like and enriched compositions, indicating a heterogeneous mantle source region consisting of enriched and depleted components. This is consistent with the assumption that a heterogeneous mantle plume, possibly the Galápagos plume, was responsible for the formation of the CLIP. The geochemically enriched and depleted components are thought to be preserved in different sized domains within the mantle plume head, together with domains of common CLIP compositions probably representing mixtures of the two components. The geochemical variability of the profiles conducted during dives with the ROV Kiel 6000 shows that these chemical heterogeneities can occur on a small scale of tens of kilometers and points to incomplete homogenization of the mantle source components in the plume head. A rough trend to more depleted compositions from older to younger samples suggests that the depleted component may have become more pronounced with time and was mainly sampled during the later episodes of magmatic activity. However, further investigations are needed to test this possible geochemical evolution in the CLIP in the central Caribbean. Our detailed sampling favors formation of the Beata Ridge through widespread extrusive magmatic activity during the main CLIP stage (95–83 Ma) with less voluminous largely intrusive activity during the second stage (81–71 Ma).

Declarations of interest

None.

Acknowledgements

We would like to thank Captain Wunderlich and Captain Baschek and the crews of the R/V Meteor for their support on board; S. Hauff, K. Junge, U. Westernströer and J. Sticklus for their analytical support; M. Anders for assistance with sample preparation and Doris Maicher for support with the volcaniclastic samples. Many thanks to David Buchs and Christopher Sinton for their constructive reviews and Andrew Kerr for editorial handling. We also thank the German Research Association (DFG) for funding the cruise and this study being part of the Ph.D. thesis of A.D. (HO1833/22-1 to K.H., R.W. and F.H.), and the GEOMAR Helmholtz Centre for funding the analytical work.

Appendix A. Supplementary data

Supplementary data to this article can be found online at https://doi.org/10.1016/j.lithos.2018.12.021.

References

Aitken, B.G., Echeverría, L.M., 1984. Petrology and geochemistry of komatiites and tholeiites from Gorgona Island, Colombia. Contributions to Mineralogy and Petrology 86, 94–105. https://doi.org/10.1007/bf00373714.

Alvarado, G.E., Denyer, P., Sinton, C.W., 1997. The 89 Ma Tortugal komatiitic suite, Costa Rica: implications for a common geological origin of the Caribbean and Eastern Pacific region from a mantle plume. Geology 25, 439–442. https://doi.org/10.1130/0091-7613(1997)025<0439:tmtksc>2.3.co;2.

Arndt, N.T., Kerr, A.C., Tarney, J., 1997. Dynamic melting in plume heads: the formation of Gorgona komatiites and basalts. Earth and Planetary Science Letters 146, 289–301. https://doi.org/10.1016/S0012-821X(96)00219-1.

Buchs, D.M., Hoernle, K., Hauff, F., Baumgartner, P.O., 2016. Evidence from accreted seamounts for a depleted component in the early Galapagos plume. Geology https://doi.org/10.1130/g37618.1.

Buchs, D.M., Kerr, A.C., Brims, J.C., Zapata-Villada, J.P., Correa-Restrepo, T., Rodríguez, G., 2018. Evidence for subaerial development of the Caribbean oceanic plateau in the late cretaceous and palaeo-environmental implications. Earth and Planetary Science Letters 499, 62–73. https://doi.org/10.1016/j.epsl.2018.07.020.

Coffin, M.F., Eldholm, O., 1992. Volcanism and continental break-up: a global compilation of large igneous provinces. Geological Society, London, Special Publications 68, 17–30. https://doi.org/10.1144/gsl.sp.1992.068.01.02.

Coffin, M.F., Pringle, M.S., Duncan, R.A., Gladczenko, T.P., Storey, M., Müller, R.D., Gahagan, L.A., 2002. Kerguelen hotspot magma output since 130 Ma. Journal of Petrology 43, 1121–1137. https://doi.org/10.1093/petrology/43.7.1121.

Courtillot, V.E., Renne, P.R., 2003. On the ages of flood basalt events. Comptes Rendus Geoscience 335, 113–140. https://doi.org/10.1016/S1631-0713(03)00006-3.

Donnelly, T.W., Melson, W., Kay, R., Rogers, J.W., 1973. Basalts and Dolerites of Late Cretaceous Age from the Central Caribbean. Initial Reports of the Deep Sea Drilling Project 15. US Government Printing Office, Washington, DC, pp. 989–1004.

Duncan, R.A., 2002. A time frame for construction of the Kerguelen Plateau and Broken Ridge. Journal of Petrology 43, 1109–1119. https://doi.org/10.1093/petrology/43.7.1109.

Duncan, R.A., Hargraves, R.B., 1984. Plate tectonic evolution of the Caribbean region in the mantle reference frame. Geological Society of America Memoirs 162, 81–94. https://doi.org/10.1130/MEM162-p81.

Duncan, R.A., Pyle, D.G., 1988. Rapid eruption of the Deccan flood basalts at the cretaceous/Tertiary boundary. Nature 333, 841–843. https://doi.org/10.1038/333841a0.

Dürkefälden, A., Hoernle, K., Hauff, F., Werner, R. and Garbe-Schönberg, D., Revised. Second-stage Caribbean large Igneous Province volcanism: the depleted Icing on the enriched Cake. Chemical Geology.

Echeverría, L.M., Aitken, B.G., 1986. Pyroclastic rocks: another manifestation of ultramafic volcanism on Gorgona Island, Colombia. Contributions to Mineralogy and Petrology 92, 428–436. https://doi.org/10.1007/bf00374425.

Escuder-Viruete, J., Pérez-Estaún, A., Contreras, F., Joubert, M., Weis, D., Ullrich, T.D., Spadea, P., 2007. Plume mantle source heterogeneity through time: Insights from the Duarte complex, Hispaniola, northeastern Caribbean. Journal of Geophysical Research: Solid Earth 112, B04203. https://doi.org/10.1029/2006jb004323.

Escuder-Viruete, J., Pérez-Estaún, A., Joubert, M., Weis, D., 2011. The Pelona-Pico Duarte basalts Formation, Central Hispaniola: an on-land section of late cretaceous volcanism related to the Caribbean large igneous province. Geologica Acta: An International Earth Science Journal 9, 307–328. https://www.redalyc.org/articulo.oa?id=50522108007.

Escuder-Viruete, J., Joubert, M., Abad, M., Pérez-Valera, F., Gabites, J., 2016. The basaltic volcanism of the Dumisseau Formation in the Sierra de Bahoruco, SW Dominican Republic: a record of the mantle plume-related magmatism of the Caribbean large Igneous Province. Lithos 254–255, 67–83. https://doi.org/10.1016/j.lithos.2016.03.013.

Fitton, J.G., Saunders, A.D., Norry, M.J., Hardarson, B.S., Taylor, R.N., 1997. Thermal and chemical structure of the Iceland plume. Earth and Planetary Science Letters 153, 197–208. https://doi.org/10.1016/S0012-821X(97)00170-2.

Frisch, W., Meschede, M., Sick, M., 1992. Origin of the central American ophiolites: evidence from paleomagnetic results. Geological Society of America Bulletin 104, 1301–1314. http://gsabulletin.gsapubs.org/content/104/10/1301.abstract.

Geldmacher, J., Hanan, B.B., Blichert-Toft, J., Harpp, K., Hoernle, K., Hauff, F., Werner, R., Kerr, A.C., 2003. Hafnium isotopic variations in volcanic rocks from the Caribbean large Igneous Province and Galápagos hot spot tracks. Geochemistry, Geophysics, Geosystems 4 (1062). https://doi.org/10.1029/2002gc000477.

Geldmacher, J., van den Bogaard, P., Heydolph, K., Hoernle, K., 2014. The age of Earth's largest volcano: Tamu Massif on Shatsky rise (Northwest Pacific Ocean). International Journal of Earth Sciences 103, 2351–2357. https://doi.org/10.1007/s00531-014-1078-6.

Golowin, R., Portnyagin, M., Hoernle, K., Hauff, F., Gurenko, A., Garbe-Schönberg, D., Werner, R., Turner, S., 2017a. Boninite-like intraplate magmas from Manihiki Plateau require ultra-depleted and enriched source components. Nature Communications 8, 14322. https://doi.org/10.1038/ncomms14322.

Golowin, R., Portnyagin, M., Hoernle, K., Sobolev, A., Kuzmin, D., Werner, R., 2017b. The role and conditions of second-stage mantle melting in the generation of low-Ti tholeiites and boninites: the case of the Manihiki Plateau and the Troodos ophiolite. Contributions to Mineralogy and Petrology 172 (104). https://doi.org/10.1007/s00410-017-1424-3.

Golowin, R., Portnyagin, M., Hoernle, K., Hauff, F., Werner, R., Garbe-Schönberg, D., 2018. Geochemistry of deep Manihiki Plateau crust: implications for compositional diversity of large igneous provinces in the Western Pacific and their genetic link. Chemical Geology 493, 553–566. https://doi.org/10.1016/j.chemgeo.2018.07.016.

Hastie, A.R., Kerr, A.C., 2010. Mantle plume or slab window?: Physical and geochemical constraints on the origin of the Caribbean oceanic plateau. Earth-Science Reviews 98, 283–293. http://www.sciencedirect.com/science/article/pii/S0012825209001767.

Hastie, A.R., Kerr, A.C., Mitchell, S.F., Millar, I.L., 2008. Geochemistry and petrogenesis of cretaceous oceanic plateau lavas in eastern Jamaica. Lithos 101, 323–343. http://www.sciencedirect.com/science/article/pii/S0024493707001764.

Hastie, A.R., Fitton, J.G., Kerr, A.C., McDonald, I., Schwindrofska, A., Hoernle, K., 2016. The composition of mantle plumes and the deep Earth. Earth and Planetary Science Letters 444, 13–25. https://doi.org/10.1016/j.epsl.2016.03.023.

Hauff, F., Hoernle, K., Tilton, G., Graham, D.W., Kerr, A.C., 2000a. Large volume recycling of oceanic lithosphere over short time scales: geochemical constraints from the Caribbean large Igneous Province. Earth and Planetary Science Letters 174, 247–263. http://www.sciencedirect.com/science/article/pii/S0012821X99002721.

Hauff, F., Hoernle, K., van den Bogaard, P., Alvarado, G.E., Garbe-Schönberg, D., 2000b. Age and geochemistry of basaltic complexes in western Costa Rica: contributions to the geotectonic evolution of central America. Geochemistry, Geophysics, Geosystems 1, 1–41. https://doi.org/10.1029/1999gc000020.

Heydolph, K., Murphy, D.T., Geldmacher, J., Romanova, I.V., Greene, A., Hoernle, K., Weis, D., Mahoney, J., 2014. Plume versus plate origin for the Shatsky rise oceanic plateau (NW Pacific): insights from Nd, Pb and Hf isotopes. Lithos 200-201, 49–63. https://doi.org/10.1016/j.lithos.2014.03.031.

Hoernle, K., Werner, R., Morgan, J.P., Garbe-Schönberg, D., Bryce, J., Mrazek, J., 2000. Existence of complex spatial zonation in the Galápagos plume. Geology 28, 435–438. http://geology.gsapubs.org/content/28/5/435.abstract.

Hoernle, K., van den Bogaard, P., Werner, R., Lissinna, B., Hauff, F., Alvarado, G., Garbe-Schönberg, D., 2002. Missing history (16-71 Ma) of the Galápagos hotspot: implications for the tectonic and biological evolution of the Americas. Geology 30, 795–798. http://geology.gsapubs.org/content/30/9/795.abstract.

Hoernle, K., Hauff, F., van den Bogaard, P., 2004. 70 m.Y. History (139-69 Ma) for the Caribbean large igneous province. Geology 32, 697–700. http://geology.gsapubs.org/content/32/8/697.abstract.

Hoernle, K., Hauff, F., van den Bogaard, P., Werner, R., Mortimer, N., Geldmacher, J., Garbe-Schönberg, D., Davy, B., 2010. Age and geochemistry of volcanic rocks from the Hikurangi and Manihiki oceanic Plateaus. Geochimica et Cosmochimica Acta 74, 7196–7219. http://www.sciencedirect.com/science/article/pii/S0016703710005430.

Hofmann, A.W., 1988. Chemical differentiation of the Earth: the relationship between mantle, continental crust, and oceanic crust. Earth and Planetary Science Letters 90, 297–314. https://doi.org/10.1016/0012-821X(88)90132-X.

Homrighausen, S., Hoernle, K., Hauff, F., Wartho, J.A., van den Bogaard, P., Garbe-Schönberg, D., 2019. New age and geochemical data from the Walvis Ridge: the temporal and spatial diversity of South Atlantic intraplate volcanism and its possible origin. Geochimica et Cosmochimica Acta 245, 16–34. https://doi.org/10.1016/j.gca.2018.09.002.

Hooper, P.R., 2000. Flood Basalt Provinces. In: Sigurdsson, H. (Ed.), Encyclopedia of Volcanoes. Academic Press, pp. 345–360.

Jackson, M.G., Cabral, R.A., Rose-Koga, E.F., Koga, K.T., Price, A., Hauri, E.H., Michael, P., 2015. Ultra-depleted melts in olivine-hosted melt inclusions from the Ontong Java Plateau. Chemical Geology 414, 124–137. https://doi.org/10.1016/j.chemgeo.2015.08.014.

Kamenetsky, V.S., Gurenko, A.A., Kerr, A.C., 2010. Composition and temperature of komatiite melts from Gorgona Island, Colombia, constrained from olivine-hosted melt inclusions. Geology 38, 1003–1006. https://doi.org/10.1130/g31143.1.

Kerr, A.C., 2005. La Isla de Gorgona, Colombia: A petrological enigma? Lithos 84, 77–101. https://doi.org/10.1016/j.lithos.2005.02.006.

Kerr, A.C., 2014. 18–Oceanic Plateaus. In: Turekian, H.D.H.K. (Ed.), Treatise on Geochemistry, Second Edition Vol. 4. Elsevier, Oxford, pp. 631–667.

Kerr, A.C., Mahoney, J.J., 2007. Oceanic plateaus: problematic plumes, potential paradigms. Chemical Geology 241, 332–353. https://doi.org/10.1016/j.chemgeo.2007.01.019.

Kerr, A.C., Saunders, A.D., Tarney, J., Berry, N.H., Hards, V.L., 1995. Depleted mantle-plume geochemical signatures: No paradox for plume theories. Geology 23, 843–846. https://doi.org/10.1130/0091-7613(1995)023<0843:dmpgsn>2.3.co;2.

Kerr, A.C., Marriner, G.F., Arndt, N.T., Tarney, J., Nivia, A., Saunders, A.D., Duncan, R.A., 1996a. The petrogenesis of Gorgona komatiites, picrites and basalts: new field, petrographic and geochemical constraints. Lithos 37, 245–260. https://doi.org/10.1016/0024-4937(95)00039-9.

Kerr, A.C., Tarney, J., Marriner, G.F., Nivia, A., Klaver, G.T., Saunders, A.D., 1996b. The geochemistry and tectonic setting of late cretaceous Caribbean and Colombian volcanism. Journal of South American Earth Sciences 9, 111–120. http://www.sciencedirect.com/science/article/pii/0895981196000314.

Kerr, A.C., Marriner, G.F., Tarney, J., Nivia, A., Saunders, A.D., Thirlwall, M.F., Sinton, C.W., 1997. Cretaceous basaltic terranes in Western Columbia: elemental, chronological and Sr-Nd isotopic constraints on petrogenesis. Journal of Petrology 38, 677–702.

Kerr, A.C., Aspden, J.A., Tarney, J., Pilatasig, L.F., 2002a. The nature and provenance of accreted oceanic terranes in western Ecuador: geochemical and tectonic constraints. Journal of the Geological Society 159, 577–594. https://doi.org/10.1144/0016-764901-151.

Kerr, A.C., Tarney, J., Kempton, P.D., Spadea, P., Nivia, A., Marriner, G.F., Duncan, R.A., 2002b. Pervasive mantle plume head heterogeneity: evidence from the late cretaceous Caribbean-Colombian oceanic plateau. Journal of Geophysical Research 107 (2140). https://doi.org/10.1029/2001jb000790.

Kerr, A.C., Pearson, D.G., Nowell, G.M., 2009. Magma source evolution beneath the Caribbean oceanic plateau: new insights from elemental and Sr-Nd-Pb-Hf isotopic studies of ODP Leg 165 Site 1001 basalts. Geological Society, London, Special Publications 328, 809–827. https://doi.org/10.1144/sp328.31.

Lapierre, H., Dupuis, V., Lépinay, B.M.d., Tardy, M., Ruíz, J., Maury, R.C., Hernandez, J., Loubet, M., 1997. Is the lower Duarte igneous complex (Hispaniola) a Remnant of the Caribbean Plume-Generated Oceanic Plateau? The Journal of Geology 105, 111–120. https://doi.org/10.2307/30079889.

Lapierre, H., Dupuis, V., Lépinay, B.M.d., Bosch, D., Monié, P., Tardy, M., Maury, R.C., Hernandez, J., Polvé, M., Yeghicheyan, D., Cotten, J., 1999. Late Jurassic oceanic crust and upper cretaceous Caribbean Plateau Picritic Basalts exposed in the Duarte igneous complex, Hispaniola: a reply. The Journal of Geology 107, 509–512. https://doi.org/10.1086/314362.

Loewen, M.W., Duncan, R.A., Kent, A.J.R., Krawl, K., 2013. Prolonged plume volcanism in the Caribbean large Igneous Province: New insights from Curaçao and Haiti. Geochemistry, Geophysics, Geosystems 14, 4241–4259. https://doi.org/10.1002/ggge.20273.

Mahoney, J.J., Coffin, M.F.E., 1997. Large Igneous Provinces: Continental, Oceanic, and Planetary Flood Volcanism. American Geophysical Union Geophysical Monograph Series. p. 438.

Mahoney, J.J., Jones, W.B., Frey, F.A., Salters, V.J.M., Pyle, D.G., Davies, H.L., 1995. Geochemical characteristics of lavas from Broken Ridge, the Naturaliste Plateau and southernmost Kerguelen Plateau: cretaceous plateau volcanism in the Southeast Indian Ocean. Chemical Geology 120, 315–345. https://doi.org/10.1016/0009-2541(94)00144-W.

Mauffret, A., Leroy, S., 1997. Seismic stratigraphy and structure of the Caribbean igneous province. Tectonophysics 283, 61–104. http://www.sciencedirect.com/science/article/pii/S0040195197001030.

Mauffret, A., Leroy, S., Vila, J.-M., Hallot, E., Mercier de Lépinay, B., Duncan, R.A., 2001. Prolonged magmatic and tectonic development of the Caribbean Igneous Province revealed by a diving submersible survey. Marine Geophysical Research 22, 17–45. https://doi.org/10.1023/a:1004873905885.

Meschede, M., Frisch, W., 1998. A plate-tectonic model for the Mesozoic and early Cenozoic history of the Caribbean plate. Tectonophysics 296, 269–291. http://www.sciencedirect.com/science/article/pii/S0040195198001577.

Pearce, J.A., 1996. In: Wyman, D.A. (Ed.), A User's Guide to Basalt Discrimination Diagrams. Trace Element Geochemistry of Volcanic Rocks: Applications for Massive Sulphide Exploration. 12. Geological Association of Canada, pp. 79–113 Short Course Notes.

Pearce, J.A., 2008. Geochemical fingerprinting of oceanic basalts with applications to ophiolite classification and the search for Archean oceanic crust. Lithos 100, 14–48. https://doi.org/10.1016/j.lithos.2007.06.016.

Pietsch, R., Uenzelmann-Neben, G., 2015. The Manihiki Plateau–a multistage volcanic emplacement history. Geochemistry, Geophysics, Geosystems 16, 2480–2498. https://doi.org/10.1002/2015gc005852.

Pindell, J., Maresch, W.V., Martens, U., Stanek, K., 2011. The Greater Antillean Arc: early cretaceous origin and proposed relationship to central American subduction mélanges: implications for models of Caribbean evolution. International Geology Review 54, 131–143. https://doi.org/10.1080/00206814.2010.510008.

Révillon, S., Arndt, N.T., Hallot, E., Kerr, A.C., Tarney, J., 1999. Petrogenesis of picrites from the Caribbean Plateau and the North Atlantic magmatic province. Lithos 49, 1–21. http://www.sciencedirect.com/science/article/pii/S0024493799000389.

Révillon, S., Arndt, N.T., Chauvel, C., Hallot, E., 2000a. Geochemical study of ultramafic volcanic and plutonic rocks from Gorgona Island, Colombia: the plumbing system of an oceanic plateau. Journal of Petrology 41, 1127–1153. https://doi.org/10.1093/petrology/41.7.1127.

Révillon, S., Hallot, E., Arndt, N.T., Chauvel, C., Duncan, R.A., 2000b. A complex history for the Caribbean Plateau: petrology, geochemistry, and geochronology of the Beata Ridge, South Hispaniola. The Journal of Geology 108, 641–661. http://www.jstor.org/stable/10.1086/317953.

Richards, M.A., Duncan, R.A., Courtillot, V.E., 1989. Flood basalts and hot-spot tracks: plume heads and tails. Science 246, 103–107. http://www.sciencemag.org/content/246/4926/103.abstract.

Serrano, L., Ferrari, L., Martínez, M.L., Petrone, C.M., Jaramillo, C., 2011. An integrative geologic, geochronologic and geochemical study of Gorgona Island, Colombia: Implications for the formation of the Caribbean large Igneous Province. Earth and Planetary Science Letters 309, 324–336. http://www.sciencedirect.com/science/article/pii/S0012821X11004262.

Sigurdsson, H., Leckie, R.M., Acton, G.D., 1997. Site 1001: Proceedings of the Ocean Drilling Program, Initial Reports 165: College Station, Texas, Ocean Drilling Program. Texas A&M University, pp. 291–357.

Sinton, C.W., Duncan, R.A., Denyer, P., 1997. Nicoya Peninsula, Costa Rica: a single suite of Caribbean oceanic plateau magmas. Journal of Geophysical Research 102, 15507–15520. https://doi.org/10.1029/97jb00681.

Sinton, C.W., Duncan, R.A., Storey, M., Lewis, J., Estrada, J.J., 1998. An oceanic flood basalt province within the Caribbean plate. Earth and Planetary Science Letters 155, 221–235. http://www.sciencedirect.com/science/article/pii/S0012821X97002148.

Sinton, C.W., Sigurdsson, H., Duncan, R.A., 2000. Geochronology and petrology of the igneous basement at the lower Nicaraguan rise, Site 1001. Proceedings of the Ocean Drilling Program: Scientific Results. Vol. 165, pp. 233–236.

Sun, S.-S., McDonough, W.F., 1989. Chemical and isotopic systematics of oceanic basalts: implications for mantle composition and processes. Geological Society, London, Special Publications 42, 313–345. https://doi.org/10.1144/gsl.sp.1989.042.01.19.

Tejada, M.L.G., Mahoney, J.J., Neal, C.R., Duncan, R.A., Petterson, M.G., 2002. Basement geochemistry and geochronology of Central Malaita, Solomon Islands, with implications for the origin and evolution of the Ontong Java Plateau. Journal of Petrology 43, 449–484. http://petrology.oxfordjournals.org/content/43/3/449.abstract.

Tejada, M.L.G., Geldmacher, J., Hauff, F., Heaton, D., Koppers, A.A.P., Garbe-Schönberg, D., Hoernle, K., Heydolph, K., Sager, W.W., 2016. Geochemistry and age of Shatsky, Hess, and Ojin rise seamounts: implications for a connection between the Shatsky and Hess Rises. Geochimica et Cosmochimica Acta 185, 302–327. https://doi.org/10.1016/j.gca.2016.04.006.

Thompson, P.M.E., Kempton, P.D., White, R.V., Kerr, A.C., Tarney, J., Saunders, A.D., Fitton, J.G., McBirney, A., 2004. Hf-Nd isotope constraints on the origin of the cretaceous Caribbean plateau and its relationship to the Galápagos plume. Earth and Planetary Science Letters 217, 59–75. http://www.sciencedirect.com/science/article/pii/S0012821X03005429.

Timm, C., Hoernle, K., Werner, R., Hauff, F., den Bogaard, P.V., Michael, P., Coffin, M.F., Koppers, A., 2011. Age and geochemistry of the oceanic Manihiki Plateau, SW Pacific:

New evidence for a plume origin. Earth and Planetary Science Letters 304, 135–146. http://www.sciencedirect.com/science/article/pii/S0012821X11000495.

Trela, J., Vidito, C., Gazel, E., Herzberg, C., Class, C., Whalen, W., Jicha, B., Bizimis, M., Alvarado, G.E., 2015. Recycled crust in the Galápagos Plume source at 70 Ma: Implications for plume evolution. Earth and Planetary Science Letters 425, 268–277. https://doi.org/10.1016/j.epsl.2015.05.036.

Trela, J., Gazel, E., Sobolev, A.V., Moore, L., Bizimis, M., Jicha, B., Batanova, V.G., 2017. The hottest lavas of the Phanerozoic and the survival of deep Archaean reservoirs. Nature Geoscience 10, 451–456. https://doi.org/10.1038/ngeo2954.

Werner, R., Hoernle, K., Hauff, F., 2011. CLIP – Origin of the Caribbean Large Igneous Province (CLIP) in Connection with the Geodynamic Evolution of the Central Caribbean. Meteor-Berichte 11–8, M81 Leg 2A/B DFG-Senatskommission für Ozeanographie, B., P. , p. 48. http://oceanrep.geomar.de/13988.

White, R.V., Tarney, J., Kerr, A.C., Saunders, A.D., Kempton, P.D., Pringle, M.S., Klaver, G.T., 1999. Modification of an oceanic plateau, Aruba, Dutch Caribbean: Implications for the generation of continental crust. Lithos 46, 43–68. https://doi.org/10.1016/S0024-4937(98)00061-9.

Wright, J.E., Wyld, S.J., 2011. Late cretaceous subduction initiation on the eastern margin of the Caribbean-Colombian Oceanic Plateau: one Great Arc of the Caribbean (?). Geosphere 7, 468–493. https://doi.org/10.1130/GES00577.1.

Please cite this article as: A. Dürkefälden, K. Hoernle, F. Hauff, et al., Age and geochemistry of the Beata Ridge: Primary formation during the main phase (~89Ma) of the Cari..., Lithos, https://doi.org/10.1016/j.lithos.2018.12.021